Frontiers in Health InformaticsISSN-Online: 2676-7104 www.healthinformaticsjournal.com
2024; Vol 13: Issue 3 Open Access

In Vivo Evaluation of a Novel Topical Formulation of Naproxen and Betamethasone Nanogel for Osteoarthritis

Avinash Kumar Rao[1*], Ruchi Tiwari[2], Naveen Gupta[3], Dharmendra Rajput[4]
[1,2,3,4]Patel College of Pharmacy, MPU, Bhopal (MP), India
*Corresponding Author: Avinash Kumar Rao
Patel College of Pharmacy, MPU, Bhopal (MP), India
avinash66rao@gmail.com

Cite this paper as: Avinash Kumar Rao, Ruchi Tiwari, Naveen Gupta, Dharmendra Rajput (2024) In Vivo Evaluation of a Novel Topical Formulation of Naproxen and Betamethasone Nanogel for Osteoarthritis. *Frontiers in Health Informatics, 13* (3), 5504-5539

A B S T R A C T
A novel topical nanogel formulation combining naproxen and betamethasone was developed and evaluated for its therapeutic potential in treating osteoarthritis (OA) using an in vivo rat model. The nanogel's pH was optimized to ensure it was suitable for skin application without causing irritation. Uniformity tests confirmed the formulation's homogeneity, with no aggregates observed. The nanogel demonstrated favorable spreadability and extrudability, crucial for effective skin application and patient compliance. The viscosity of the formulation was also assessed, revealing ideal properties for stable and consistent use. Rats were induced with OA via intra-articular injection of monosodium iodoacetate (MIA), leading to joint pain, inflammation, and reduced mobility. A significant decrease in motor coordination was observed using a rotarod apparatus, highlighting the detrimental effects of OA on joint function. The weight-bearing distribution between the affected and healthy limbs was evaluated using an in-capacitance tester, revealing improvements in the nanogel-treated groups. Additionally, the arthritis index (AI) score, which accounted for swelling and limping, showed a steady decline over time in nanogel-treated rats. Inflammatory cytokine levels were measured in the serum, showing a reduction in inflammation in treated groups. In vivo skin safety evaluations indicated that the nanogel caused no significant skin irritation. Paw volumes were also monitored throughout the study, demonstrating decreased inflammation in the nanogel-treated group compared to controls. The novel naproxen and betamethasone nanogel exhibited promising therapeutic benefits in reducing OA symptoms, including pain, inflammation, and impaired mobility, while maintaining a favorable safety profile for topical use. This formulation holds potential for further development as an effective topical treatment for osteoarthritis.

Keywords: osteoarthritis, nanogel, naproxen, betamethasone, inflammation

INTRODUCTION

Osteoarthritis (OA) is a degenerative joint disorder affecting millions of people worldwide, characterized by the progressive degradation of cartilage, joint inflammation, and pain(Allen, Thoma, and Golightly 2022). It is one of the most common forms of arthritis, often leading to disability and a reduced quality of life for those affected(Paget et al. 2023). Although OA can impact any joint, it primarily affects weight-bearing joints such as the knees, hips, and spine. As a multifactorial disease, OA arises from a combination of genetic, metabolic, and mechanical factors, with aging and obesity being significant contributors(Oteo Álvaro 2021). Current therapeutic strategies for OA are largely focused on managing symptoms, reducing pain, and improving joint function, rather than addressing the underlying causes of cartilage degeneration. Among these therapies, nonsteroidal anti-inflammatory drugs (NSAIDs) like naproxen and corticosteroids such as betamethasone play a pivotal role in pain relief and inflammation control(Hinman et al. 2023).
Naproxen, a commonly used NSAID, exerts its therapeutic effects by inhibiting the cyclooxygenase (COX) enzymes, specifically COX-1 and COX-2, which are involved in the production of prostaglandins that mediate

inflammation and pain(Heidari-Beni et al. 2020). By reducing the levels of prostaglandins, naproxen helps to alleviate the discomfort associated with OA(Karateev, Lila, and Alekseeva 2021). However, despite its efficacy, systemic administration of naproxen is often associated with gastrointestinal complications, including ulcers and bleeding, as well as cardiovascular risks. These adverse effects limit its long-term use, particularly in elderly patients who are more susceptible to these complications(Munir et al. 2023).

Betamethasone, on the other hand, is a potent corticosteroid that works by inhibiting multiple inflammatory pathways, including the suppression of pro-inflammatory cytokines and the inhibition of leukocyte migration to inflamed tissues(Y. Wang et al. 2023). Corticosteroids like betamethasone are often used for short-term relief of severe OA symptoms, particularly when NSAIDs are insufficient(Y. Wang et al. 2022). However, repeated systemic administration of corticosteroids can lead to significant side effects, such as immunosuppression, osteoporosis, and adrenal suppression, which restrict their long-term application in OA management(Inagaki et al. 2022). Consequently, there is a growing interest in developing topical formulations that can deliver these drugs directly to the affected joints, minimizing systemic exposure and reducing the risk of adverse effects(H. Yang et al. 2022).

The concept of using nanotechnology in drug delivery has gained substantial attention in recent years, particularly in the field of topical formulations(Freitas et al. 2021). Nanogels, which are nanosized hydrogel particles, represent an innovative drug delivery system with several advantages over conventional formulations(Sobhani, Li, and Cortes 2023). These include enhanced drug solubility, increased drug stability, controlled drug release, and improved penetration of the drug through the skin. Nanogels can encapsulate both hydrophilic and hydrophobic drugs, offering versatility in formulating a wide range of therapeutic agents. Moreover, the small size of nanogels allows for better interaction with biological tissues, potentially improving the bioavailability of drugs at the site of action(Sakib, Verma, and Islam 2022).

In the context of OA treatment, a nanogel formulation could offer several potential benefits. By delivering NSAIDs and corticosteroids directly to the joint via topical application, it may be possible to achieve effective local concentrations of the drugs while minimizing systemic absorption and thereby reducing the risk of side effects(Pan et al. 2023). Furthermore, nanogels can be engineered to provide sustained release of the encapsulated drugs, prolonging their therapeutic effects and reducing the frequency of application. This is particularly advantageous in managing chronic conditions like OA, where long-term pain control is essential for improving patient quality of life(Joshi and Phansopkar 2022).

The rationale for combining naproxen and betamethasone in a single nanogel formulation stem from their complementary mechanisms of action. While naproxen primarily targets the COX enzymes to reduce prostaglandin-mediated inflammation, betamethasone exerts broader anti-inflammatory effects by modulating immune responses and inhibiting multiple inflammatory pathways(Jin et al. 2020). By using these two drugs in combination, it may be possible to achieve more effective control of OA-related pain and inflammation than with either drug alone. Furthermore, the use of a nanogel as the delivery vehicle could enhance the penetration of both drugs through the skin and into the deeper tissues of the joint, where they are needed most(Pergolizzi et al. 2020).

Several studies have explored the use of nanotechnology-based drug delivery systems for OA, with promising results. For example, nanoparticle-based formulations of NSAIDs have been shown to enhance drug penetration through the skin and reduce inflammation in animal models of arthritis(Ramos-Inza et al. 2024). Similarly, corticosteroids encapsulated in nanoparticles have demonstrated improved efficacy and reduced side effects in preclinical studies(Bella Triana and Anan Suparman 2022). However, to date, few studies have examined the potential of combining NSAIDs and corticosteroids in a single nanogel formulation for OA treatment(Sobhani et al. 2023).

The development of a topical nanogel formulation containing both naproxen and betamethasone represents a novel approach to OA management, with the potential to offer superior therapeutic outcomes compared to conventional treatments(Jadhav and Erande 2023). In addition to reducing pain and inflammation, such a formulation could provide several other benefits, including improved patient compliance and convenience(Salmons et al. 2023). Unlike oral medications, which must be taken regularly and can cause gastrointestinal discomfort, a topical nanogel can be easily applied to the affected joint, offering a non-invasive

and potentially more acceptable treatment option for patients(Dell'Isola et al. 2022).
The present study aims to evaluate the in vivo efficacy of a novel topical nanogel formulation containing naproxen and betamethasone in an animal model of OA. The primary objectives are to assess the ability of the nanogel to reduce joint inflammation and pain, as well as to examine the pharmacokinetics of the formulation to determine the extent of systemic absorption of the drugs. Secondary objectives include evaluating the safety of the nanogel formulation, particularly with respect to any local or systemic adverse effects(Munir et al. 2023).

PREPARATION OF NAPROXEN NANOSUSPENSIONS

Materials and methods

Naproxen and PVP was once bought from Lobe Chemie, Pvt. Ltd. (Mumbai). Sodium Alginate and HPMC E15 was purchased from Modern Science, Nashik. Tween 80 procured from Corneal, France(Ramos et al. 2023).

Pre-formulation studies

The purpose of pre-formulation testing is to examine the characteristics of a drug material both on its own and when combined with excipients. Utilising pre-formulation parameters increases the likelihood of creating a product that is legal, safe, effective, and stable while also laying the groundwork for improving the quality of the medicinal product(Nupur et al. 2023).

Melting point analysis

The melting point for the obtained naproxen sample was tested using open capillary method. Before conducting the analysis, the equipment was calibrated. Subsequently, the drug sample was compressed into capillary tubes, each having dimensions of 6 mm in length and 1 mm in diameter(Medeiros, Ferreira, and Cavalheiro 2023). These capillaries were then inserted vertically into the equipment with a heating rate maintained at 10 °C per minute. The readings were collected in triplicate, and the drug's melting point was documented, followed by a comparison with the melting point of a reference sample(Ayorindea, Agbolabori, and Odeniyia 2023).

Determination of λmax for naproxen

UV spectroscopic analysis was employed to determine the wavelength (λmax) at which the naproxen sodium. The drug was accurately weighed and dissolved in a solvent to generate a stock solution with a concentration of 1000 µg/ml. Following this, the solution underwent suitable dilution using the same solvent, resulting in a concentration of 100 µg/ml. The UV spectrum of this concentration was then documented across the wavelength range of 200–400 nm. It is important to highlight that the UV spectrum of the drug was acquired using a methanol solven(Mirocki et al. 2022)t.

Standard curve of naproxen using UV-visible spectrophotometric method

A calibration curve for naproxen was established by creating serial dilutions from a 0.1 mg/ml stock solution within the range of 2-12 µg/ml). Spectrophotometric analysis of the prepared samples was conducted at λmax 272 nm in the specified medium. The absorbance-concentration relationship was plotted (Zhou et al. 2021.

Drug-polymer compatibility by analytical techniques of naproxen nanosuspensions

Fourier transform infrared spectroscopy (FTIR)

FTIR study is essential to determine the purity and interaction between different drugs and polymers. Therefore, I.R. spectra of Naproxen and blends of drug and polymers were monitored compared to KBr tablet using a Shimadzu – 8700 FTIR spectrophotometer. For this test, plain KBr and drug-polymer blends in potassium bromide discs were prepared by intimate mixing in a glass mortar pestle. Then, the prepared mixtures were punched into a transparent tablet using special dies under high pressure. Finally, the prepared tablets were placed in an I.R. spectrometer (FTIR-8700, Shimadzu) to record the spectrum(Rojek, Gazda, and Plenis 2023).

Differential Scanning Calorimetry

Differential Scanning Calorimetry analysis of the naproxen drug sample involved precisely weighing a small amount (2-3 mg) of naproxen, which was then carefully placed in an aluminum pan. The pan was hermetically sealed using a crimper, and the sample pan, along with a reference pan, was introduced into the DSC analyzer. It underwent heating from 40°C to 400°C range. The process was carried out under an inert atmosphere, with flow rate of 100 ml/min(Nupur et al. 2023).

Similarly, DSC analysis of the naproxen drug sample in combination with polymers such as PVP, sodium alginate, and HPMC E15 was conducted using the same procedure. A small amount of the naproxen and polymer mixture (2-3 mg) was accurately weighed, sealed in an aluminum pan, and subjected to the DSC analyzer. The heating process, inert atmospheres, and other conditions were consistent with those employed for the individual naproxen sample analysis(Quddus et al. 2023).

Selection of stabilizers

Water-soluble stabilisers from the surfactant and polymer classes were chosen because they make it simpler than their hydrophobic equivalents for poorly soluble medicines to create an aqueous dispersion with them. To investigate their impact on the stability of nanosuspension, a total of three stabilisers from the literature (Table.1) were chosen. Initially, several batches of nanosuspensions were made solely using polymeric stabilisers such sodium alginate, HPMC E15, and PVP(Fatih Dilekoglu and Yapici 2023). Researchers looked at the lowest quantity of stabilisers needed to assist the size reduction and stabilise the nanosuspension in order to prevent toxicity caused by their surface-active capabilities. The findings produced by stabilisers were used to choose the stabilisers to be used in nanosuspension. To create various stabiliser solutions, precisely weighed quantities of stabilisers (polymer/surfactant) were added and dissolved in distilled water(Yeganeh et al. 2022).

Table. 1: Screened stabilizers and their ratio to the drug for preparing naproxen nanosuspensions.

Code	Drug: Polymer ratio
N1	1:0.5 (Naproxen: PVP)
N2	1:1 (Naproxen: PVP)
N3	1:1.5 (Naproxen: PVP)
N4	1:0.5 (Naproxen: Sodium alginate)
N5	1:1 (Naproxen: Sodium alginate)
N6	1:1.5 (Naproxen: Sodium alginate)
N7	1:0.5 (Naproxen: HPMC E15)
N8	1:1 (Naproxen: HPMC E15)
N9	1:1.5 (Naproxen: HPMC E15)

Method of Preparation

Naproxen nanosuspension is prepared by antisolvent precipitation method using various stabilizers concentrations such as PVP (N 1, N 2, & N 3), Sodium alginate (N 4, N 5, & N6), and HPMC E15 (N 7, N 8, & N 9) in the ratio of 0.5, 1 and 1.5 % respectively, and in all the formulation naproxen (1%) and co-stabilizer Tween 80 volume remain constant (Table 3.2). On the basis of literature review, details were finalized for pre-formulation studies. Drug Naproxen is dissolved in methanol (5ml) at room temperature(Medeiros et al. 2022). The procedure involved the gradual addition of the organic solution of the drug, delivered via a plastic syringe in drops, into an aqueous solution containing a stabilizer at a controlled rate of 0.5 mL/min. The subsequent dispersion underwent stirring at 500 rpm for 6 minutes and was subsequently subjected to sonication for a duration of 5–10 minutes. Double-distilled water was used with very slow rate and introduced into the dispersion, with continuous stirring for an additional hour. This step facilitated, eventually resulting in the removal of the organic solvent i.e., methanol was removed by evaporation by keeping it at 50°C leading to the formation of nanosuspension. Naproxen is insoluble in water that's why it is precipitate with

stabilizer(Sharapova et al. 2021).

Table 3.2: Composition of various batches of naproxen nanosuspension.

Formulation code	Ingredients					
	Drug (mg)	Methanol (ml)	PVP 100 (mg)	Sodium alginate (mg)	HPMC E15 (mg)	Tween 80 (ml)
N 1	200 mg	5	100	-	-	0.5
N 2	200 mg	5	200	-	-	0.5
N 3	200 mg	5	300	-	-	0.5
N 4	200 mg	5	-	100	-	0.5
N 5	200 mg	5	-	200	-	0.5
N 6	200 mg	5	-	300	-	0.5
N 7	200 mg	5	-	-	100	0.5
N 8	200 mg	5	-	-	200	0.5
N 9	200 mg	5	-	-	300	0.5

Formulation of dry nanoparticles

Shelf life of the suspension can be extended to understand the nature of dissolution, the naproxen nanosuspensions were freeze dried. At the time of lyophilization, cryoprotectant was added (1% mannitol) in all formulations. Nanosuspension was lyophilized using a Virtis freeze dryer. The sample was initially stored for one night at -70 °C in a deep freezer, and subsequently for two days at -50 °C at 2 millitorr in a virtis freeze dryer(Ma et al. 2021).

Evaluation of Naproxen Nanosuspension Formulations

Particle size and size distribution

The determination of particle size was conducted through photon correlation spectroscopy (PCS) using the Zetasizer 3000 instrument from Malvern Instruments, UK. This analytical method provided the mean diameter (z-average) within a measuring range of 20–1000 nm. All presented data represent the mean values obtained from three independent samples manufactured under consistent production conditions(Zare and Mehrabani-Zeinabad 2022).

Zeta Potential

The analysis of zeta potential in the naproxen nanosuspension formulation was performed using the Zetasizer 3000 instrument from Malvern Instruments. Prior to measurement, the samples underwent dilution with de-ionized water and were placed in an electrophoretic cell, where an electrical field of 15.2 V/cm was applied. Each sample was then subjected to analysis to determine its zeta potential value(Ye et al. 2022).

Scanning Electron Microscopy

The morphology of shape, cross-section, and surface of pure Naproxen and nanosuspension formulations of naproxen with PVP, sodium alginate, and HPMC E15 were monitored by the SEM system called Phenom Pro Desktop (Phenom 1481), Thermo Fisher Scientific, USA(Arslan et al. 2024).

Drug content

The nanosuspensions that were prepared underwent drug content analysis using the UV spectroscopic method. Various batches of nanosuspensions, each equivalent to 10 mg of naproxen, were accurately weighed and dissolved in 50 ml of methanol. The naproxen content in the samples was analyzed after appropriate dilution using a double-beam UV spectrophotometer (model UV-1700, Shimadzu, Japan) at the wavelength λmax 272 nm. This procedure was conducted in triplicate, and the averages were subsequently calculated(Aljubailah et al. 2022). Drug content was calculated by the following equation

$$\text{Drug content } \% = \frac{\text{Observed drug content}}{\text{Theoretical drug content}} \times 100$$

Entrapment efficiency

Centrifugation was performed for fifteen minutes at 11,000 rpm on newly developed nanosuspension aliquots containing 10 mg of naproxen. By using UV testing on the supernatant, the amount of disintegrated medication was determined. Using an ultraviolet (UV) spectrophotometer that was set to 272 nm, the amount of medication present in the clear residue after centrifugation was measured(Wibrianto et al. 2021). The following formula was used to calculate the % of drug entrapment efficiency:

$$\text{entrapment efficiency } = \frac{\text{quantity of drug encapsulated in the formulation}}{\text{Total quantity of drug in the formulation}} \times 100$$

Research on In-Vitro Drug Release

The USP dissolving test device with the paddling technique, revolving at a speed of 50 rotations per minute(rpm), was used for the in-vitro dissolving investigations of both pure naproxen and its nanosuspension. Dissolution profiling was conducted in a recently made 7.4 pH phosphate buffer solution. The cellophane membrane was submerged in the dissolving mixture for 12 hours before the start of the experiment(X. Wang et al. 2022). Then, a cellophane tube containing naproxen nanosuspension (equal to ten milligrams (mg) of naproxen) was submerged in the dissolving media. The dissolving media was 37.0 ± 0.2 °C in temperature and had an amount of 900 ml. At prearranged intervals, materials were removed, and fresh buffer was added in an equivalent volume. Spectrophotometric measurements of the removed samples' absorbance at 272 nm were made. Every determination was made three times. The release profile of the pure medication was compared with the data obtained for various preparation batches(Jalil, Chowdhury, and Laman 2023).

Kinetics and mechanism of drug release

Numerous kinetic models exist that explain how drugs generally release from dose formulations. To clarify the release rate and its mechanics, model-dependent approaches were researched(Reddyy et al. 2024)s. The following forms of data treatment were used to plot the in-vitro profile results for each formulation:

1. Zero-order kinetic model: tracking the total proportion of medication released over time.
2. First-order kinetic model: the cumulative proportion of medication remaining shown against time using a logarithmic approach.
3. Higuchi's model: A graph showing the total amount of medication released in time squared.
4. Korsmeyer equation: displaying the logarithm of the total amount of medication released as a function of time.

Results and Discussion

Preformulation studies

Preformulation research, such as analytical study, analytical technique selection, and preliminary formulation trials, must come before the formulation development activity. The information from preformulation studies reduces issues in subsequent stages of the creation of naproxen nanosuspension and lays the foundation for successful formulation attempts, which lowers the cost of producing developed products.

Appearance of the drug

The organoleptic characteristics of the sample of medicine were examined; it was found to be white in color, odorless, and non-hygroscopic. (Table.3).

Table.3: Pharmacopoeial specifications on organoleptic characteristics of Naproxen

Drug	Properties	Standard Value or USP/IP specifications	Observed Value
Naproxen	Description	White or white crystalline	White crystalline powder
	Odour	Odourless	Odourless
	Solubility	Easily dissolves in ethanol and methanol, but has limited solubility in water	Complies

Determine the melting point.

It was decided what the melting point of the obtained naproxen sample was. The drug substance's melting point was found to be 153.1°C (Table.4) using the capillary method, which is within the range that has been reported in the literature. A decrease in melting point as well as a broadening of the melting point range in the presence of relatively modest amounts of impurities. The readings' proximity to the stated value, however, shows that the substance has been correctly identified and there are no impurities.

Table.4: Melting point (MP) determination

Drug	Theoretical MP (°c)	Observed MP (°c)			Average (°c)
		I	II	III	
Naproxen	153°C	153	153.2	153.1	153.1± 0.1°C

Determination of λ_{max} for naproxen

The naproxen mixture in phosphate buffer at pH 7.4 showed maximum absorbance at 232 and 272 nm in its UV spectrum, as seen in the image that goes with it. Figure.1

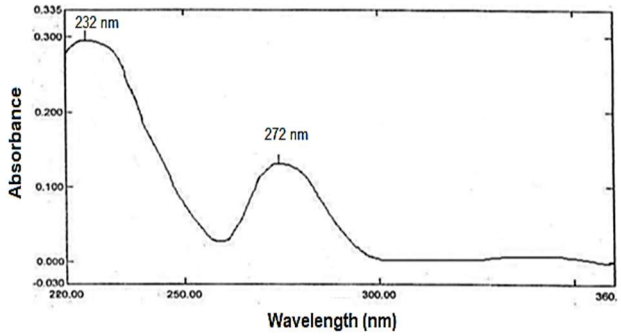

Figure 1: UV spectra of naproxen drug

Naproxen standard curve in pH 7.4 phosphate buffer

The absorbance and naproxen concentration have a linear relationship as indicated by calibration curves (Figure 2). The absorption peaks at 272 nm, which followed Beer's law in the range of 2–12 µg/ml, were revealed by the U.V. spectrophotometric quantitative quantification of naproxen (Table 5). With a correlation value (R2) of 0.9955, the linear regression equation Y = 0.1772x + 0.1799 is displayed in Figure 2.

Table 5: pH 7.4 phosphate buffer with Naproxen calibration curve data

Concentration (µg/ml)	Absorbance			Average N=3 (±SD)
2	0.364	0.368	0.361	0.364 ± 0.121

4	0.542	0.548	0.549	0.546 ± 0.182
6	0.687	0.682	0.686	0.685 ± 0.228
8	0.873	0.877	0.879	0.876 ± 0.292
10	1.082	1.088	1.086	1.085 ± 0.362

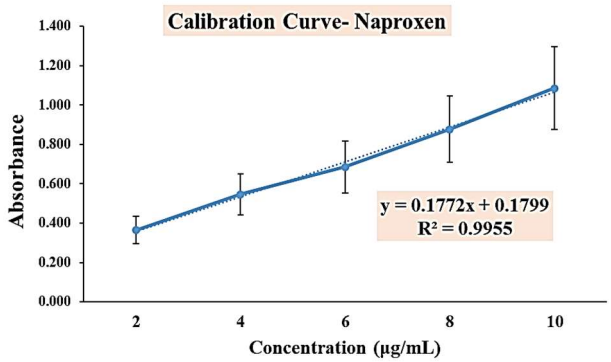

Figure 2: Calibration curve of naproxen

Drug-polymer compatibility by analytical techniques

Drug-polymer compatibility analyses and practical investigations aim to swiftly define any actual or prospective interactions between naproxen and other formulation ingredients. In the early stages of formulation development, it is a crucial exercise in risk minimization. The stability and/or bioavailability of pharmaceuticals can change due to drug-excipient incompatibility, which might impact their safety or efficacy.

Fourier transform infrared spectroscopy (FTIR)

Compatibility assessments were conducted using an FTIR spectrophotometer. In the FTIR spectrum (depicted in Figure 3.6), notable peaks were observed, including C−H stretching vibrations at 3004 & 2967 cm-1, C−O stretching vibrations at 1029 cm-1, aromatic C=C stretching vibrations at 1605 & 1438 cm-1, and CH3 bending vibration at 1395 cm-1, indicative of the characteristic features of naproxen. The OH bond and the C-H (benzene ring) were connected to absorption peaks at 3217 cm-1 and 820 cm-1, respectively, whereas etheric bonds were linked to peaks at 1265, 1158, and 1029 cm-1. A physical combination of naproxen with PVP, sodium alginate, and HPMC E15 is also shown in Figure 3.7, along with its FTIR spectra. There were no additional new peaks, and the locations of the absorption bands in the spectra did not alter, indicating that there were no substantial interactions between naproxen and the polymers.

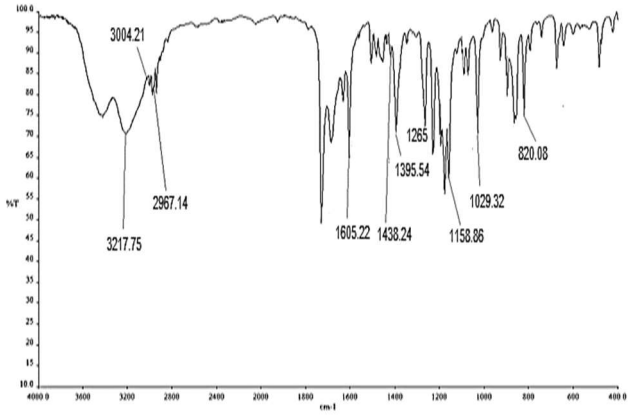

Figure 3: Naproxen's FTIR spectrum

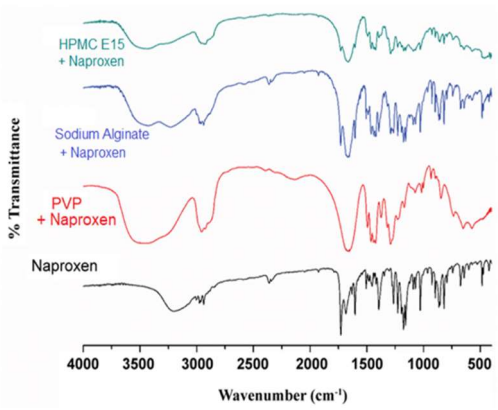

Figure 4: Physical mixes of naproxen with PVP, sodium alginate, and HPMC E15, as well

as naproxen's FTIR spectra.

Differential calorimetry scanning

The naproxen DSC thermogram is shown in Figure 3.8. The pure drug's melting point, or its unique endothermic peak, was confirmed by DSC experiments at 153.5°C. To evaluate possible interactions between the medication and polymers, the DSC thermogram of physical mixes comprising naproxen and other polymers was given in Figure 3.9. These mixes' DSC thermograms, which showed strong endothermic peaks at 151.9°C, 152.7°C, and 153°C, respectively, closely matched the drug's melting point of 153.5°C. The mixtures included PVP, sodium alginate, and HPMC E15. This implies that the medicine and selected excipients did not interact in any noticeable way.

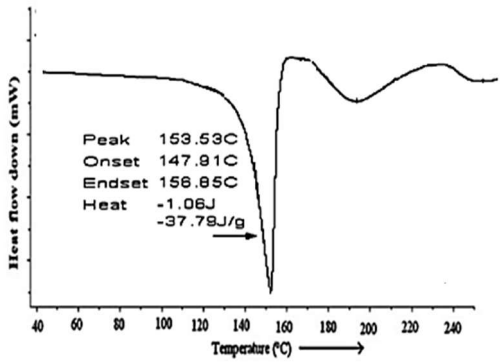

Figure 5: DSC thermogram of naproxen

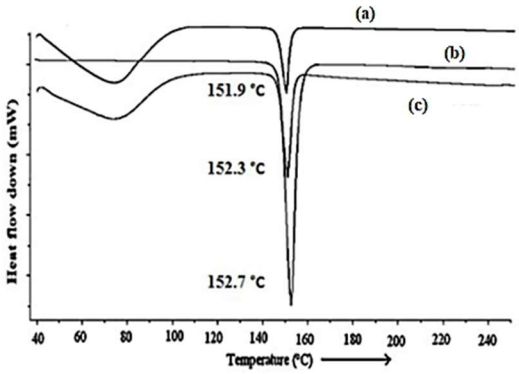

Figure 6: Naproxen physical combination with (a) PVP, (b) sodium alginate, and (c) HPMC E15 polymer thermograms of DSC

Evaluation of naproxen nanosuspension formulations

Particle size and size distribution

Quality indicators including solubility, dissolution, bioavailability, and content homogeneity are all strongly affected by particle size. While the drug's particle shape affects surface area, compaction force, and flow characteristics. Spherical shape molecules have the most surface area and have a uniform flow property, compared to molecules with oval, angular, needle, and rough forms. Because a larger surface area provides greater solubility, BCS Class II medicines increase solubility by decreasing the particle size.

Table 6: The polydispersity index, zeta potential, and mean particle size of the nanosuspension

Sr. No.	Batch code	Mean Particle size (nm)	PDI	Zeta potential (mV)
1.	N1	185.2 ± 0.33	0.516 ±0.41	-12.6±0.23
2.	N2	193.0 ± 0.37	0.459 ± 0.11	-16.8±0.09
3.	N3	215.9 ± 0.26	0.327± 0.22	-17.3±0.19
4.	N4	100.6 ± 0.28	0.265 ± 0.21	-1.67±0.09
5.	N5	106.3 ± 0.21	0.595 ± 0.16	-16.6±6.27
6.	N6	144.5 ± 0.13	0.393 ± 0.13	-9.56±3.14
7.	N7	129.0 ± 0.13	0.422± 0.26	-18.6±2.97
8.	N8	110.7 ± 0.64	0.318 ±0.21	-26.9±0.3
9.	N9	133.8 ± 0.15	0.424 ± 0.16	-22.5±5.73

The prepared nanosuspension showed nano size range from 100.6 to 215.9 nm and poly dispersity index range from 0.265 to 0.595 (Table 3.6). It signifies a favorable consistency in the particle size distribution, highlighting the importance of selecting appropriate stabilizers and determining their concentrations for effective size and stability control. Among the nine formulations examined, all fall within the typical nano size range. Notably,

formulations coded as N4 and N5, incorporating sodium alginate, as well as N8 with HPMC E15, exhibited particularly reduced particle sizes. Furthermore, the PDI of formulations N4 (0.265 ± 0.21) and N8 (0.318 ±0.21) were also found good as compared to other formulations. Therefore, it is possible that N4 and N8 formed a homogeneous suspension upon reconstitution, and the low PDI value will suggest that the nanosuspension is stable.

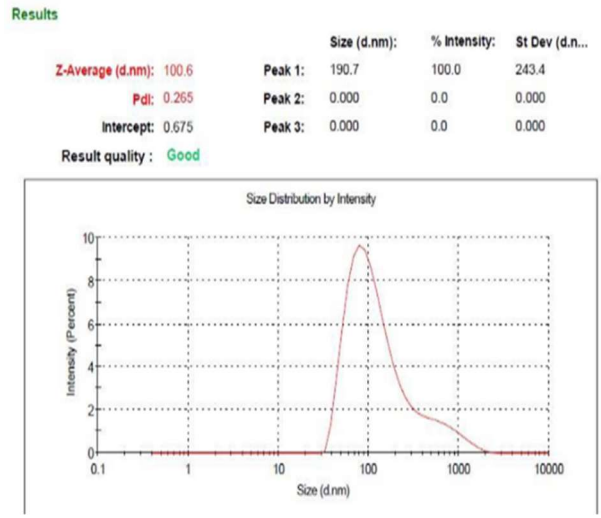

Figure 7: The polydispersity index and particle size of the nanosuspension N4.

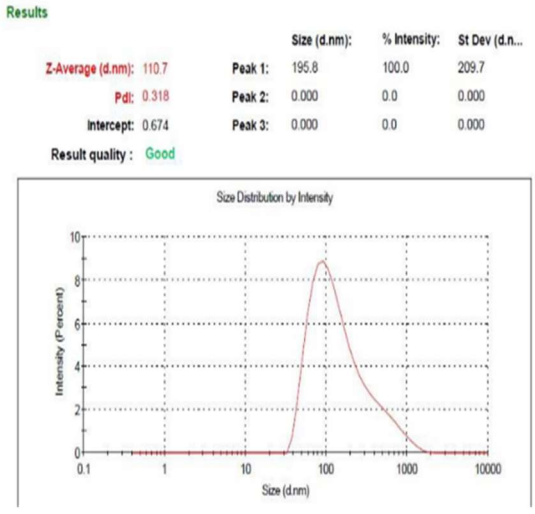

Figure 8: Size of particles and polydispersity index of the N8 nanosuspension.

Table 6 showed average particle size of all formulations which demonstrated that the proportion of medication to excipient concentration affects particle size of nanosuspensions. The hydrophobicity of the polymer chain in the instance of PVP employed in this study is what causes polymer adsorption on hydrophobic surfaces. On the other hand, the polymer's hydrophilic moiety engages with the medium. Chain morphology is therefore essential for steric stabilisation and polymer adsorption. Particularly long-swinging hydrophilic chains seem to offer higher steric stability and aggregation resistance. It has been discovered that increasing the polymer content in the nanosuspension formula causes the drug particle size to rise. This result might be explained by the drug particles aggregating as a result of too much polymer being added, which resulted in an accumulation of thick layers that covered the drug particles. The same is true for sodium alginate-based nanosuspensions. Because the alginate molecule is bulky, reducing the polymer concentration consequently decreases the particle size.
The HPMC E15-made nanosuspensions, on the other hand, showed a clear pattern. The following reasons may explain why the dimensions of the particles decreased as the concentration of HPMC E15 was increased from 0.5% to 1.0%. Because HPMC is a nonionic polymer, precipitation was less likely. Because of the hydrodynamic boundary layer surrounding the nanosuspensions and the polymer molecules' adsorption on the growing crystal faces, HPMC provides a steric hindrance to the clumping and growth of nanosuspensions. The drug-stabilizer system may be explained by the hydrogen bonds that form between the drug molecules and the stabilizer, which has a large number of hydroxyl groups. Although, the source of the rise in particle size and further increases in HPMC E15 concentration from 1.0% to 1.5% may be the solution's increased viscosity, which may impede the diffusion between the solvent and antisolvent during precipitation formation. Greater particle size was produced as a result of Ostwald ripening. Furthermore, the deposition of concentric layers of HPMC on the drug surface resulted in larger particle sizes. The formulation that provided the greatest steric repulsion between crystals and enough surface coverage was found to have a concentration of 1.0% W/V HPMC.

Zeta Potential Analysis

By determining the particles' electrophoretic movement in an electric field, the zeta potential of a colloidal

system—which represents the particle charge—was determined. High-energy surfaces are produced when nanoparticles are produced, if proper stabilisation does not occur. Eventually, aggregates, the Ostwald ripening process, and an unstable colloidal dispersion result from this. Stabilisation becomes increasingly important when the particle size decreases and the free surface energy increases. Both the manufacturing of nanosuspensions and storage stability depend on stability. Zeta potential has significantly affected the storage stability of colloid dispersion systems by representing the electrostatic obstacles that may stop nanoparticles from agglomerating and clustering. It is desirable to have a zeta potential of at least -20 mV for sterically stabilised systems or -30 mV for electrostatically stabilised systems in order to produce a physically stable nanosuspension. Due to the presence of negatively charged PVP, sodium alginate, and HPMC in the current investigation, the naproxen nanosuspension's zeta potential (Table 6) was discovered to have negative values, and the observed zeta potential was low (-1.67 to -26.9 mV). The HPMC E15 based formulation (N8) showed zeta potential value of -26.9 mV (Figure 9) which suggest that the method selected for development and optimization produced a stable nanosuspension formulation.

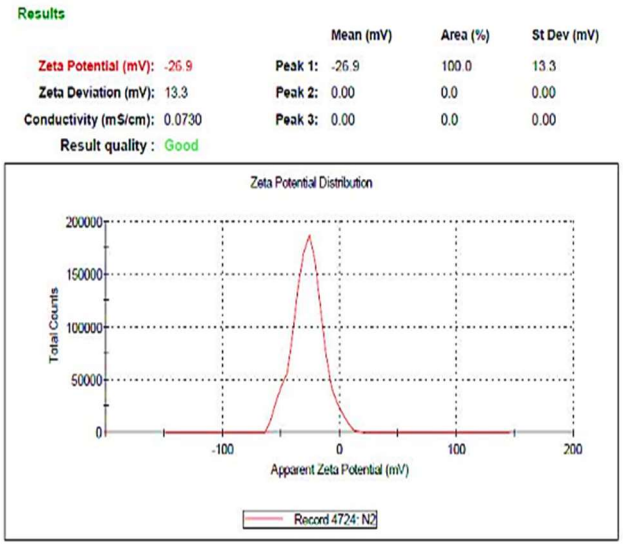

Figure 9: Zeta potential of N8 nanosuspension

Particles with sufficient zeta potential to provide a sufficient steric or electric barrier are less likely to aggregate. It is important to note that the adsorption of a steric stabilizer, like the HPMC in formulations (N7-N9) in our study, reduces the measured zeta potential. This is because the HPMC's layer of adsorption on the medication surface, where the zeta potential is measured, has caused the drug surface to become further away from the plane of shear.

Scanning Electron Microscopy

For surface morphology characterization of nanosuspension formulations, SEM images of the pure drug were contrasted with SEM images of the nanosuspension formulations, captured immediately after preparation, as illustrated in Figure 10. The micrographs vividly revealed substantial distinctions between the raw crystal form of naproxen and the nanosuspensions. The former exhibited a large and irregular structure (Figure 10), whereas in the nanosuspension, the particle size markedly diminished, assuming a spherical shape, possibly due to the presence of a polymeric coating on the particles (Figure 10b-d)

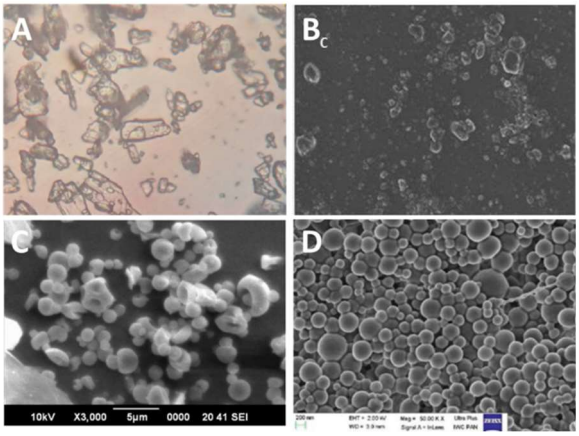

Figure 10: Optical microscopic images of naproxen crystal (a); SEM of naproxen nanosuspensions, (b) naproxen HPMC nanosuspension, (c) naproxen PVP nanosuspension, and (d) naproxen sodium alginate nanosuspension

Drug Content Determination

The developed nanosuspension formulations' drug content examination produced good results, with uniform distribution seen in every formulation. As shown in Table 7, the percentage of medications varied from 87.35±2.48% to 95.12±3.96%. The presented data indicates that the formulated naproxen nanosuspension exhibited high drug content with low standard deviation, signifying minimal drug loss during the preparation process. This suggests a consistent and effective dispersion of the drug within the powder formulation. Notably, among the formulations, HPMC E15-based nanosuspension (N8) exhibited a particularly high percentage of drug loading, enhancing the clinical feasibility of drug delivery.

Table 7: The percentage of drug content and entrapment efficiency in nanosuspension preparations.

Sr. No.	Batch code	Entrapment efficiency (%)	Drug content (%)
1.	N1	74.37±1.76	87.35±2.48
2.	N2	81.65±1.98	88.05±1.23
3.	N3	79.13±2.04	92.72±2.92
4.	N4	73.69±1.73	89.95±1.28
5.	N5	80.45±3.01	93.48±2.10
6.	N6	78.56±2.72	91.34±3.56
7.	N7	80.43±2.73	89.34±2.99
8.	N8	84.0±1.48	94.12±3.96
9.	N9	81.81±2.31	95.45±3.71

Value shown as mean ± SD for n = 3.

The increase in the percentage of drug content with an increase in polymeric concentration can be explained by the formation of extra concentric layers of polymeric molecules on the drug surface, which prevent the drug from diffusing back into the bulk.

Estimation of Entrapment Efficiency of Nano-suspension

The data was calculated and mentioned in Table 7. The naproxen entrapment efficiency of N8 (84.0 ± 1.48 %) was high when compared to other nanosuspension formulations.

The most important aspect affecting entrapment efficiency is the stabiliser concentrations utilised. It could be as a result of the surfactant's ability to lessen friction at the polymer-aqueous phase contact.

Studies on In-Vitro Release

Naproxen nanosuspension's in vitro drug release profile was studied for 12 hours. The data are shown in Figure

10. Pure naproxen dissolved at a relatively slow pace. After 12 hours, only 24.82% of the medication was liberated in phosphate buffer. However, naproxen nanosuspensions dissolution rate was increased more than the pure naproxen. The different nanosuspension formulations showed the drug release in vitro in the range between 59.80% to 99.80%. This may be as a result of the drug's larger surface area and/or potential improved interaction between the nanosuspensions and dissolving media. Naproxen's sluggish rate of dissolution may be due to its large crystal size, however the nanosuspensions exhibited significantly faster rates of dissolution, which may be explained by the following causes. (a) High hydrophilicity polymers improve wettability, decrease aggregation, and become locally soluble by the carrier in the diffusion layer, increasing the rate of dissolution, As the drug dissolves more quickly in its amorphous form than in its crystalline form due to a higher thermodynamic activity, (b) the naproxen-loaded nanosuspensions generated from polymers exhibit a reduction in crystallinity.(c) The formulation's naproxen dissolution rate may accelerate due to the larger surface area and resulting smaller particle size.

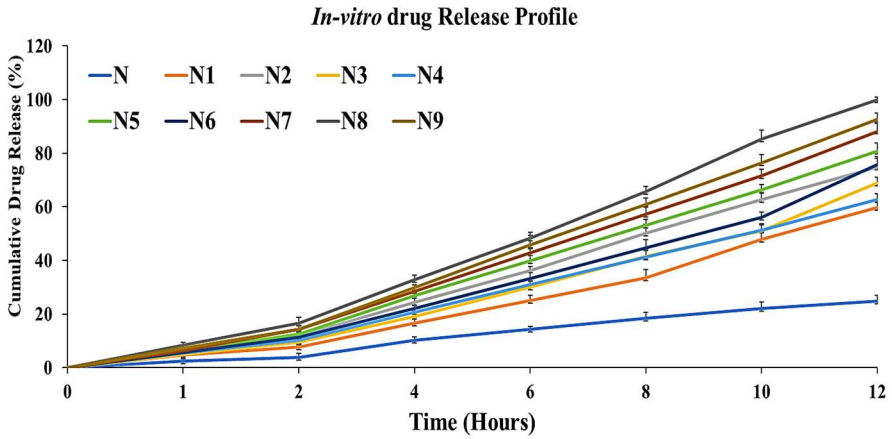

Figure 10. The in vitro release profile of formulations including nanosuspension and pure naproxen

Based on the above data, HPMC E15 based nanosuspension formulation (N8) showed maximum *in-vitro* release i.e. 99.80 % (in phosphate buffer) drug was released at the end of 12 hrs with increasing carrier proportion. Since the drug molecules were totally entrapped inside the gel structure, the change in diffusion layer thickness caused by HPMC's gel formation action is what is responsible for the variance in release rate in different formulations of HPMC E15 (N7-N9). The hydrophilicity of HPMC in the higher drug-HPMC ratios presumably had an impact on this outcome. Additionally, the high concentration of HPMC might raising the viscosity, and thereby the higher concentration of anti-nucleant, which resulted in a reduction in drug release.

Kinetics and mechanism of drug release

To comprehend the process of drug release and release rate kinetics of the drug from nanosuspension, the data from the in-vitro drug release was fitted to a variety of mathematical models, including zero and first order, Higuchi (matrix), and korsemeyer-peppas. The R2 values, or regression coefficient, are listed in Table 8. The drug release in the control sample followed a diffusion-controlled mechanism, according to the correlation coefficient analysis. The fact that the first-order (0.9903) 'r' values are greater than the zero-order (0.9895) and Higuchi's square root of time (0.8991) indicates this. As a consequence, the data indicated that the first-order release pattern predominated over the others. Even so, the results showed that the drug release from all nanosuspension formulations followed zero order kinetics, as indicated by the higher value of "r" for zero order (in the range of 0.9854 to 0.9998) compared to first order (in the range of 0.9832 to 0.9995). Additionally, the Korsemeyer-Peppas equation was used for the drug release mechanism. All the formulation was having good linearity when checked with Korsmeyer-peppas model. The *n* value for the control sample was found as 0.891, which indicated that the release kinetics follows case-II transport/ zero order, i.e., swelling controlled drug

release. This kinetics explained that the diffusion process taken place at quicker rate in comparison to the relaxation process and the system is further controlled by relaxation ($R_{diff} >> R_{relax}$,). In contrast, the values of n in the case of nanosuspension formulations ranged from 1.010 to 1.025, indicating that n > 0.89 was observed. This suggested that the release of the drug kinetics followed super case-II transit, meaning that the drug was released by both polymer chain relaxation (Rrelax) and diffusion (Rdiff), and it also suggested that the drug might be released as a result of chain disentanglement and hydrophilic polymer swelling.

Table 8: Release kinetics data for control naproxen and nanosuspension formulations.

Formulation code	Regression coefficients (R^2)			
	Zero order	First order	Peppas	Higuchi
Control (N)	0.9895	0.9903	0.9943 n = 0.891	0.8991
N1	0.9854	0.9832	0.9956 n = 1.208	0.8159
N2	0.9996	0.9991	0.9998 n = 1.025	0.8659
N3	0.9996	0.9884	0.9962 n = 1.151	0.8302
N4	0.9998	0.9995	0.9998 n = 1.010	0.8711
N5	0.9997	0.9992	0.9998 n = 1.019	0.8676
N6	0.9907	0.9888	0.9948 n = 1.125	0.8373
N7	0.9994	0.9986	0.9997 n = 1.031	0.8643
N8	0.9991	0.9982	0.9993 n = 1.025	0.8662
N9	0.9996	0.9989	0.9999 n = 1.030	0.8644

Conclusions

The use of nanosuspensions offers a workable solution to the problems caused by naproxen's poor solubility, which has frequently reduced its therapeutic efficacy. By employing several stabilisers in varying amounts, including PVP, sodium alginate, and HPMC E15, different nanosuspensions containing naproxen was created. DSC and IR spectrum analyses revealed that the medication and the formulation ingredient were compatible. All experiments were performed including *in-vitro* drug release experiments were performed on each formulation. To compare the process of drug release from various formulations to that of pure drugs, in vitro release rates were studied for nanosuspension formulations. Furthermore, formulation N8 was chosen as the best formulation with the requisite attributes based on a variety of assessment metrics. Naproxen nanosuspension prepared by using HPMC E15 as stabilizer was considered as the best because of its good stability as zeta potential of -26.9 mV, mean particle size diameter as of 110.7 nm, drug content of 94.12%, entrapment efficiency of 84%, and *in-vitro* drug release data displayed 99.80% of drug release rate profile up to 12 h. This investigation made it clear that HPMC E15 performed better than the other evaluated polymers at accelerating naproxen dissolution. The drug solubility and dissolution rates of the nanosuspension made with HPMC E15 showed significant improvements, enhancing bioavailability and perhaps improving therapeutic results. The ratio of medication to polymer also significantly impacted Zeta potential, particle size, and entrapment efficiency. Contrary to traditional medications, the nanocarrier system may make some medications more soluble and shield them from circulating oxidation, enhancing their local bioavailability and lowering unfavourable side effects. It is crucial to remember that more study and research may be necessary to completely comprehend the underlying mechanisms and improve the formulation process for nanosuspension.

BETAMETHASONE SODIUM PHOSPHATE LOADED CHITOSAN ALGINATE NANOPARTICLES

Materials & Equipment

Fourrts India in Chennai, India sent a complimentary sample of betamethasone sodium phosphate (BSP). We purchased sodium alginate and chitosan from the Sigma-Aldrich Chemical Company in the United States(Li et al. 2022). Calcium chloride, potassium dihydrogen phosphate, and sodium hydrogen phosphate were purchased from Adwik, El Nasr Pharmaceutical Chemical Company in Egypt. The tools employed in the investigation

include the following: transmission electron microscopy ([Joel 100CX], Japan), FT-IR spectrophotometer (Genesis II Mattson, USA), Malvern Nanoseries ZetaSizer (Nano-ZS90, 633 nm He-Ne 200), and a sonicator(Kianersi et al. 2021).

Methods

Preparation of blank chitosan-alginate nanoparticles

The preparation process used here for the nanoparticle's formulation is called ionotropic-gelation. The process has been adapted from existing literatures and involves two steps. The solutions of chitosan and sodium alginate were made by mixing the polymers with distilled water. Making use of hydrochloric acid. The required amount of chitosan was dissolved in 1% lactic acid solution to produce the required chitosan concentrations. The chitosan solutions were adjusted to a pH of 5.2 ± 0.2 by adding 1 M sodium hydroxide(Ahmad et al. 2022). The required amount of calcium chloride was dissolved in distilled water to create calcium chloride solutions, which were then produced to the required concentrations. The process of producing nanoparticles begins with the production of pre-gel. After 30 minutes of stirring at 400 rpm, 10 ml of a 0.5% (w/v) sodium alginate solution and 6 ml of a 0.5% aqueous calcium chloride solution were combined. The second step included constantly stirring the calcium alginate pre-gel for 30 minutes while adding 4 millilitres of a 0.08% w/v chitosan solution (pH 5.2). The resultant opalescent dispersion was left to settle at room temperature for an entire night to facilitate the formation of homogenous particles by nanoparticles(Kianersi et al. 2021).

Formulation of nanoparticles encapsulating betamethasone sodium phosphate within a chitosan-alginate matrix

To achieve the appropriate concentrations (0.2, 0.4, 0.6, 0.8, and 1.0%), the required amounts of BSP were mixed with sodium alginate solutions, and the same procedure was used for the placebo(Kolding et al. 2023). A varied quantity of medication, ranging from 0.2% to 1.0%, was added to the organic phase to achieve maximal encapsulation in order to assess the impact of drug amount in the nanoparticles. As a solubilizing agent, tween 80 (0.5%), a non-ionic surfactant, was utilized to further prevent the aggregation of nanoparticles. Table 1 below displays the composition of the produced formulations. After allowing the nanoparticles to form homogenous particles by adjusting the resultant opalescent solution overnight, the effects of different BSP concentrations on the formulations' encapsulating performance, zeta potential, particle size, and in-vitro release were evaluated(Selmin et al. 2022).

Table 1: Composition of BSP loaded chitosan alginate nanoparticles

Formulation code	Na Alginate concentration % w/v	Tween 80 concentration % w/v	BSP concentration % w/v	$CaCl_2$ concentration % w/v	Chitosan concentration % w/v
B1	0.5	0.5	0.20	0.5	0.08
B2	0.5	0.5	0.40	0.5	0.08
B3	0.5	0.5	0.60	0.5	0.08
B4	0.5	0.5	0.80	0.5	0.08
B5	0.5	0.5	1.0	0.5	0.08

Concentration in polymer solution, (total volume = 20 ml)

Characterization of the Prepared BSP Loaded Chitosan Alginate Nanoparticles:

Quantitative Analysis

BSP was assayed using UV spectrophotometer (Shimaduz, USA). BSP was dissolved in distilled water to create a BSP solution (10 µg/ml). By measuring the absorbance of various BSP solution concentrations, a calibration curve was formulated(Ivković et al. 2023).

Determination of the encapsulating efficiency

The amount of drug entrapped in the NPs was determined by deducting the total amount of BSP used in the NPs' production from the total amount of drug that was still disseminated in the water-based suspending medium but wasn't entrapped(Campos et al. 2024). Five millilitres of BSP-loaded NP mixtures were centrifuged at 6000 rpm for thirty minutes to extract the drug-loaded nanoparticles from the water-based solution (supernatant) containing unloaded BSP. UV spectrophotometer (UV spectrophotometer; Shimaduz, USA) was used, the supernatant was analysed for the presence of free drugs at 246 nm. As shown below, the drug entrapment efficiency was determined.

$EE\% = [(A - B)/A] \times 100$

The total quantity of drug in the nano dispersion is represented by A, while the free amount of drug in the supernatant is shown by B(Y. Yang et al. 2022).

Determination of Average particle size and distribution

The Zetasizer 2000 (Malvern Instruments Ltd., UK) was utilised to perform dynamic light scattering (DLS) in order to measure particle size and polydispersity index (PDI). For three hours, 200 µg of lyophilized nanoparticles were reconstituted in 2 mL of 0.2 µm filtered water to guarantee the complete dissolution of big aggregates(Biswasroy et al. 2024). After 20 seconds of vortexing, the re-suspended particles were sonicated for 15 minutes to help break them up, vacuum filtered (10 µm particle retention) to remove any remaining excess polymer, and sonicated for an additional 5 minutes before being transferred to disposable polystyrene cuvettes with a 1 cm path length and put in the analyser. The study was carried out at 25 °C, with an angle of scattering of 90° and a refractive index of 1.590. Particle size was expressed in terms of z-average size (intensity) for each sample, and the average diameter and standard deviation were assessed in triplicate(X. Wang et al. 2023).

Determination of Zeta potential

The Zetasizer 2000 from Malvern Instruments Ltd., UK, was used to calculate the zeta potential of the nanocarrier dispersion. This was accomplished by diluting the 0.25 ml nanocarrier dispersion with a distilled solution before adding it to the electrophoretic cell. Based on the collected mean electrophoretic mobility data, the zeta-potential values were computed(Shalaby, El-Gazayerly, and Abdallah 2022).

Determination of Morphology of chitosan-alginate nanoparticles

Transmission electron microscopy (Joel 100CX, Japan) was used to examine the morphology of nanoparticles (NPs). For analysis, a copper grid was coated with a single drop of chitosan-alginate nanosuspension containing BSP, which was then left to dry at room temperature(Mohamed et al. 2021).

FT-IR analysis

In order to examine any connections between BSP and chitosan/alginate, Fourier-transform infrared (FT-IR) spectra were collected. FT-IR spectroscopy was used to record the FT-IR spectra for BSP, ALG, CS, and the physical mixture of BSP, ALG, and CS (Genesis II Mattson, USA). A 2% weight/weight sample was combined with dry potassium bromide (KBr) and crushed into a fine powder using an agate mortar(Timotijević et al. 2022). A 10,000 psi hydraulic press was then used to compress the mixture into KBr discs. Using IR solution software, each KBr disc was scanned at 4 mm/s and 2 cm resolution throughout a wave number range of 400–4000 cm-1. This allowed for the identification of unique peaks for the different samples(Mashoofnia, Mohamadnia, and Kompany-Zareh 2021).

Determination of *In-vitro* release profile

For the in-vitro experiment, cellophane barrier was employed in many BSP NP preparations (30/32). A test tube (diameter 0.4 cm) with open ends was attached with the cellophane barrier on one side. To touch the cellophane membrane, one millilitre of the synthesized nanoparticles was introduced from the other side. The receptor storage space, which held 10 ml of hot distilled water in a beaker at 37°C, submerged the whole membrane(Rastegar Ramsheh et al. 2021). A magnetic stirrer maintained constant agitation of the receptor compartment at 200 rpm. At designated intervals of 1, 2, 4, 6, 8, and 12 hours, a specified volume (1 ml) of the

solution from one millilitre of brand-new, distilled water was added to the receptor region after it was removed. The drug content of the withdrawn samples was measured using a UV spectrophotometer calibrated to 246 nm against free BSP drug. Additionally, free BSP drug was tested for in vitro release as a reference, and samples were collected at the same intervals as the BSP-loaded nanoparticles(Riccio et al. 2021)

Statistical analysis

Every experiment was run in triplicate as an independent experiment, and the data is shown as mean + standard deviation (SD). The statistical analysis was conducted using Sigma Plot v. 11 software (San Jose, California, United States), with a p-value of less than 0.05 being considered statistically significant. ANOVA, or one-way assessment of variance, was employed to assess the significance of the variations among the variables. When suitable, 95% confidence-level linear correlation and covariance estimation were carried out(Tam et al. 2023).

Results and Discussion

UV spectral analysis of BSP

The UV absorption spectrum of the BSP solution was examined, revealing its peak absorbance at 246 , illustrated in Figure1.

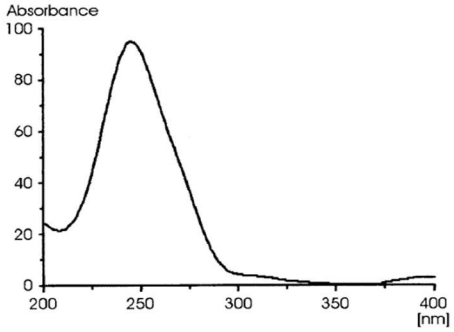

Figure 1: UV spectrum of betamethasone sodium phosphate.

Construction of standard curve

Calibration curves show a linear relationship as presented (Figure 2). The U.V. spectrophotometric quantitative estimation of BSP showed the absorption maxima at 246 nm, which obeyed Beer's law in the range of 10-20 µg/ml (Table 2). Linear regression equation Y = 0.0894X + 0.3857 with correlation coefficient (R^2) of 0.9665 (Figure 2).

Table 2: Calibration curve data of BSP in distilled water

Sr. No.	Conc. (µg/mL)	Absorbance
1	10	0.432
2	12	0.580
3	14	0.694
4	16	0.765
5	18	0.823
6	20	0.898

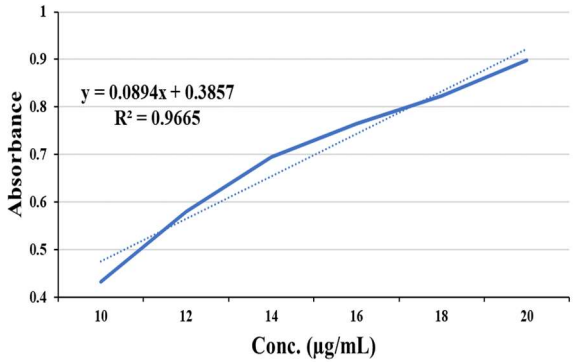

Figure 2: Calibration curve of BSP in distilled water

Determination of Encapsulation efficiency

Different drug concentrations (0.2%, 0.4%, 0.6%, 0.8%, and 1%), as well as zeta potential and encapsulation efficiency, were developed to investigate the effects of changing BSP concentrations. The measured range of encapsulation effectiveness for several BSP formulations was 66.72% to 69.29%. Furthermore, there was a little downward trend in the encapsulation efficiency (from about 69.29% to roughly 66.72%) when the amount of medication in the formulation rose (Figure 3). It was found that the encapsulating efficiency was somewhat reduced as the drug concentration was raised (Table 3). Drug-polymer interactions in the polymer have an impact on the drug content in nanoparticles. Increased drug incorporation is correlated with increased drug miscibility

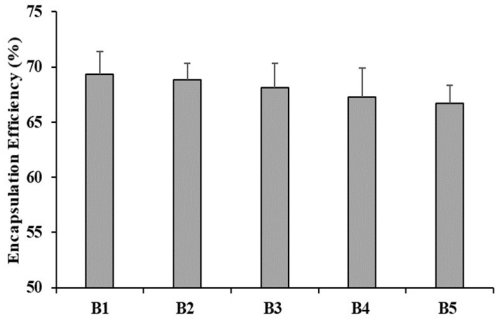

Figure 3: Encapsulation efficiency (%) of different BSP loaded nanoparticle formulations

The decline in encapsulation efficiency with higher drug content in the formulation could be attributed to the heightened propensity of the drug to diffuse into the external solution. According to earlier research, adding more dexamethasone to chitosan tripolyphosphate nanoparticles reduces the loading efficiency because the medication diffuses into the external solution.

Table 3: Particle size, zeta potential and encapsulating efficiency of different BSP loaded nanoparticle formulations

Formulation code	Average Particle Size (nm)	Zeta Potential (mV)	Encapsulation Efficiency (%)
B1	148.49± 20.3	+ 18.21	69.29 ± 2.12
B2	142.31 ± 18.2	+ 19.73	68.83 ± 1.52
B3	131.64 ± 26.6	+ 21.48	68.09 ± 2.25
B4	125.57 ± 15.7	+ 23.44	67.24 ± 2.66
B5	110.7 ± 12.4	+ 26.90	66.72 ± 1.63

Particle size analysis

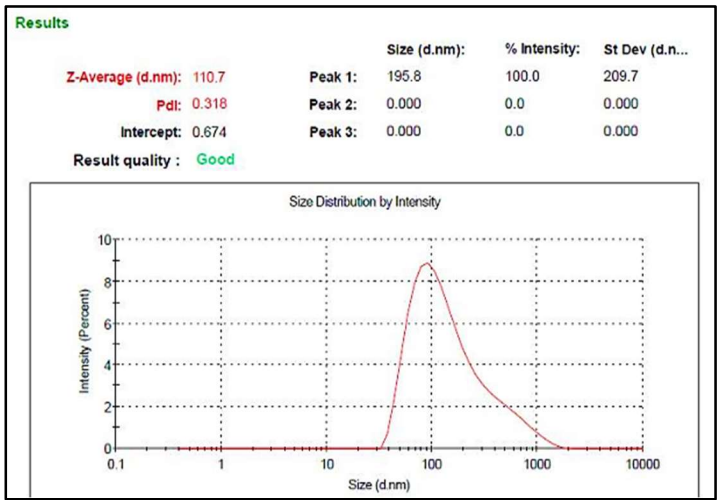

Figure 4: Particle size distribution of B5 formulation

The BSP loaded NP formulations' average particle sizes were found to be in the range of 110.70 and 148.49 nm (Table 4.3), with formulation B5 demonstrating the best nanoparticle formulation with an average size of 110.7 nm and a polydispersity index (PDI) of 0.318 (Figure 4.8). The PDI score is <1.0, indicating that the particles are distributed uniformly. The primary determinants of nanoparticle size were average value (nm) and size variability. The relative variance of the distribution was represented by the unitless variable known as the PDI, which was used to assess size variability. In other words, the uniformity of the distribution of nanoparticle sizes is symbolised by the PDI. They are necessary to keep colloidal dispersion stable and prevent the production of precipitates or tiny particles. The uniform particle size distribution and low value of PDI might be the result of improved formulation variables.

Zeta potential analysis

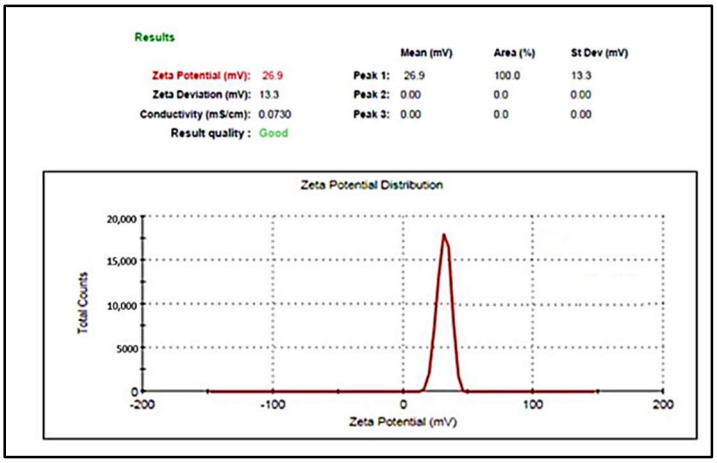

Figure 5: Zeta potential of B5 formulation

As an important particle property that affects both particle longevity and cell binding, the zeta potential value is significant. All BSP NP formulations were found to have zeta potentials between +18.21 and +26.90 mV (Table 3), among which formulation B5 showed good zeta potential of +26.90 mV as shown in Figure 5. While possessing a positive surface charge, BSP-loaded alginate-chitosan nanoparticles exhibit sufficient repulsive force to deter aggregation during prolonged storage.

The overall charge on nanoparticles produced by the ionotropic pregelation process includes Ca^{2+} ions. The core/shell structure of the nanoparticles created by this method is thought to be what distinguishes them from other types. The core is a molecule that is located between the protonated-NH3+ of CS, the Ca+2 ions of CaCl2, and the COO- groups of ALG. Furthermore, the excess Ca+2 ions that separate in the outermost coating of the nanoparticles and do not disintegrate into the polyelectrolyte complex provide on the outside a net positive charge.

Morphological examination

Transmission electron microscopy (TEM) analysis of the produced nanoparticles revealed that they were spherical particles with a solid structure. The nanoparticles, however, had a fluffy look rather than a flat surface (Figure 6). The nanoparticles' shape matched that of the chitosan-alginate nanoparticles produced by ionotropic gelation found in earlier research. However, these particles were significantly smaller when analyzed with TEM observed with the zetasizer. The zeta sizer, according to Parbha et al., measures the apparent size (hydrodynamic radius) of particles, including hydrodynamic barriers around aqueous particles like CS and ALG. As a result, the size of the NP may be overestimated.

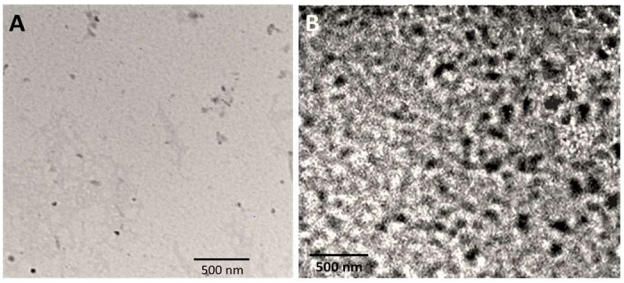

Figure 6: TEM photomicrograph of (A) BSP loaded nanoparticles and (B) Chitosan-alginate nanoparticles

Since spherical NPs have a higher surface area to volume ratio than other shapes, they have a more reactive surface and, as a result, more opportunities to have a therapeutic effect. Because of this, spherical NPs become yet another important element of NP morphology.

FTIR analysis

Only after a comprehensive analysis of the physicochemical characteristics of the drug and polymers can a formulation be developed. A proper formulation requires compatibility between the drug and the polymer. The FT-IR spectroscopy provides the potential information on how the drug and polymer interact.

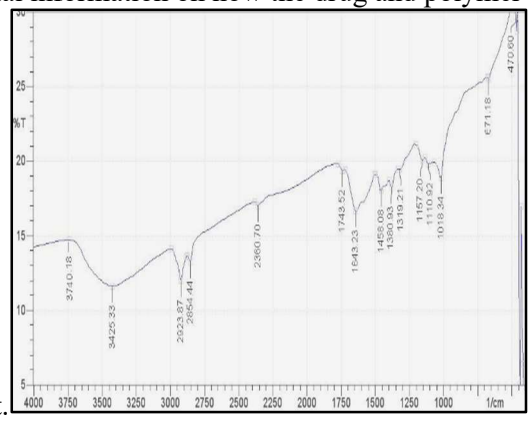

Figure 7: FT-IR Spectrum of Chitosan

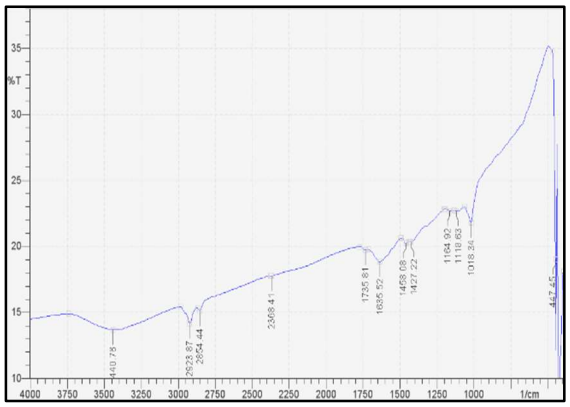

Figure 8: FT-IR Spectrum of Sodium Alginate

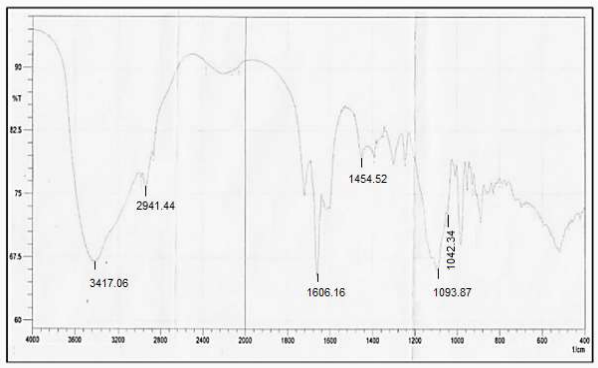

Figure 9: FTIR spectrum of betamethasone sodium phosphate

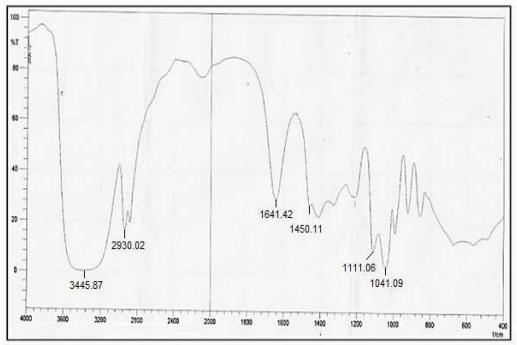

Figure 10: FTIR spectrum of physical mixture of BSP, sodium alginate and chitosan

The large bands in the chitosan spectrum (Figure 7 at 3425 cm-1 and 3740 cm-1, respectively, represent the amine and hydroxyl groups. The amide I band (the carbonyl group (C=O) stretching secondary amide) is shown by the absorption band at 1643 cm-1, the amide II band (the N-acetylated residues) is visible at 1591 cm-1, and the peak at 2854 cm-1 is the consequence of -OH stretching. The amide and ether bond N-H stretching and the amide II band N-H stretching are responsible for the peaks at 1458 and 1380 cm-1, respectively. C-O-C stretching and primary OH (the distinctive peak of –CH2-OH in primary alcohol, C-O stretch) are shown by the peaks at 1110 and 1018 cm-1. Bands at 1018 cm-1 (C-O-C stretching) in the alginate spectrum (Figure 8) correspond to its saccharide structure. The asymmetric and symmetric stretching peaks of carboxylate salt groups are responsible for the peaks at 1427 and 1458 cm-1. Furthermore, C=O stretching and C-H stretching (aliphatic) are responsible for maxima at 1735 and 2923 cm-1, respectively.

The wide band at 3417 cm-1 in the betamethasone sodium phosphate spectrum (Figure 9) represents free hydroxyl groups, while the peak at 2941 cm-1 is caused by -OH stretching. The secondary hydroxyl group (typical peak -CHOH in cyclic alcohols, C-O stretch) and primary -OH (typical peak -CH2-OH in primary alcohol, C-O stretch) are responsible for the peaks at 1093 and 1042 cm-1, respectively. The asymmetrical and symmetrical stretching of carboxylate salt groups is attributed to the 1606 and 1454 cm-1 bands.

The band at 3100 to 3500 cm-1 grows wide in the infrared spectra of the physical mixture of betamethasone sodium phosphate with excipients (Figure 10), suggesting improved hydrogen bonding. Certain distinct peaks associated with chitosan and alginate disappear or become weaker as a result of interactions including hydrogen bonding and electrostatic interactions.

In vitro drug release profile

The bioavailability and in vitro drug release of BSP-loaded nanoparticles can both be impacted by their particle size (Figure 11). Chitosan may absorb significant amounts of water due to its hydrophilic nature before undergoing hydrolysis, erosion, and other types of breakdowns that release the therapeutic chemicals. According to the findings of the release study, maximal drug release (67.08%) occurs in 12 hours for the formulation with the highest drug concentration (B5), compared to 6 hours for nearly 100% in vitro release for pure BSP. As a result, it was discovered that the percentage release of free drug BSP was greater than that of combination BSP-Alg-CS nanoparticles. It is possible that the cross-linked polymer will function as a barrier to the medium's penetration, delaying the breakdown and diffusion of the drug ingredient into the medium, which would further delay the drug release. Additionally, the composites' electrostatic connection enabled the drug to diffuse slowly from the polymeric matrix, enabling the prolonged release. The drug has a regulated release profile because of its enhanced diffusional distance and the surrounding polymeric network's obstructive properties.

In addition, increasing the BSP concentration from a low to a high level led to a higher percentage of drug release during a 12-hour period, varying from 60.20% to 67.08%. A comparatively less quantity of polymer in

the formulation may be the cause of the increased release rate and total amount released at 12 hours, since it may prevent the medication from diffusing from the nanoparticles. Furthermore, every formulation demonstrated a biphasic release pattern, which is defined by a quick release at first, followed by a longer-lasting release. The presence of free drug in the nanosuspension and on the surfaces of the nanoparticles was thought to be the cause of the first release of BSP. These results are consistent with past studies, which showed that nifedipine was released from chitosan-alginate nanoparticles in a controlled and continuous way following an initial burst. The burst release may be helpful in achieving a therapeutic concentration quickly. The therapeutic concentration is then maintained via the continuous release. In addition to the medication dissolving in the release medium, the particles expanding, and a minor degree of hydrolytic degradation/erosion of the CS matrix, release is mostly driven by the API molecules diffusing out of the NPs.

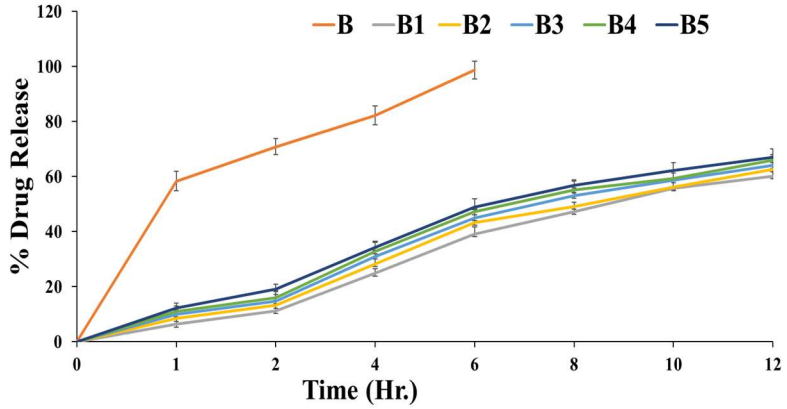

Figure 11: Influence of Betamethasone Sodium Phosphate (BSP) Concentration on the in Vitro Release Profile from Chitosan-Alginate (CS-ALG) Nanoparticles

Optimization of the formulations

The ionotropic pregelation approach was determined to be appropriate for the manufacture of BSP loaded ALG/CS nanoparticles based on the physicochemical parameters of the ALG/CS formulations as all formulations developed in the form of nanoparticles with sustained-release features. Additionally, B5 was chosen as the best NP formulation for future research among all formulations due to its small particle size (110.7 nm), it is believed to enhance the ability of particles to penetrate through biological barriers. Additionally, B5 had the highest positive zeta potential (+26.9 mV), indicating robust mucoadhesion and good colloidal stabilization of the NPs against clotting.

Conclusions

In this investigation, we illustrated a method for the synthesis of novel biodegradable nanoparticles containing betamethasone sodium phosphate (BSP). These nanoparticles were loaded into cross-linked chitosan-alginate matrices using the ionic gelation method, aiming to optimize therapy for osteoarthritis (OA). The synthesized nanoparticles were thoroughly characterized for their suitability in biomedical applications. The use of nanoparticles might offer a workable solution to the problems caused by fast dissolution of drug, which thereby may provide less residence time, and ultimately reduced its therapeutic efficacy. The ionic gelation process was utilised to successfully manufacture betamethasone sodium phosphate (BSP) loaded nanoparticles. The BSP-loaded nanoparticles underwent in vitro drug release experiments, entrapment efficiency assessments, and physicochemical characterisation. Compatibility between the drug and formulation components was shown by Fourier-transform infrared (FTIR) spectrum analysis. Each formulation underwent extensive evaluations, which included in vitro drug release assays, zeta potential measurement, drug content estimation, entrapment efficiency evaluation, and particle size analysis. Formulation B5 was then found to be the best option as it met all of the evaluation criteria and had the necessary qualities. The combined results demonstrated the safe and

efficient release of BSP from B5 nanoparticles, highlighting their potential use in the management of common and long-term diseases like osteoarthritis (OA).

PREPARATION OF NANOGEL BY COMBINATION OF NAPROXEN AND BETAMETHASONE NANOPARTICLES

Materials and Methods

We purchased triethanolamine, glycerine, acetone, and carbopol 940 from Modern Science, Nashik. The materials used were all obtained straight from the manufacturer, without further purification or inspection, and were of analytical reagent (AR)/laboratory reagent (LR) quality or the highest possible grades(Samiraninezhad et al. 2023).

Preparation of topical nanogel containing naproxen and BSP nanoparticles

The nanogel containing naproxen and BSP nanoparticles was prepared using membrane emulsification technique. This process involves pressurizing the dispersed phase and delivering it into the steady state through a microporous barrier to create droplets from two different, immiscible liquids. The process variables and composition were established by a previously published procedure. In this study, the dispersed phase was taken as the dispersion of naproxen NPs and BSP NPs in acetone, and is passes through the ceramic membrane, which have uniform pore size (100-200 nm)(Ciurba et al. 2023). The required quantity of the naproxen NPs and BSP NPs were added in acetone in a 1:1 ratio to give a final concentration of 1.0% of naproxen and BSP in the gel. Emulsion droplets or microgels are generated on the membrane surface, and subsequently, the prepared emulsion droplets or microgels are recovered as the continuous phase passes through the membrane. To achieve this, a carbopol gel was prepared by dispersing the required amount of carbopol 940 (0.5% w/v) into a small quantity of double-distilled water, left aside for 24 hours to achieve uniform swelling(Chettupalli et al. 2023). This dispersion served as the continuous phase. The resulting emulsion droplets were obtained in an oil-in-water (O/W) configuration, with the membrane pore size regulating the size of the prepared droplets and the transmembrane pressure. Additionally, 5.0% glycerin was incorporated as a humectant, and the pH of the nanogel was adjusted to approximate skin pH by adding a few drops of triethanolamine (0.05%). Furthermore, the mixture was allowed to stand overnight to eliminate entrapped air and facilitate the conversion of polymer cross-linking into a gel(Srividya et al. 2022).

Evaluation of Physicochemical properties of topical nanogel

Determination of pH

A digital pH metre (Electrolab, Bombay, India) was used to measure the topical nanogel's pH. One gramme of the topical nanogel was added to a 50millilitre beaker that already had 20 millilitres of filtered water before the measurement was done. The topical nanogel was submerged in the pH metre electrode, and the pH reading was noted(Afshar et al. 2024).

Homogeneity

Using a topical nanogel's visual examination, homogeneity research was conducted. The synthesised topical nanogel was poured into vials of flint colour and submitted to ocular inspection to see if it was homogeneous and if aggregates were present or not(Yang et al. 2023).

Determination of Spreadability & Extrudability

The spreadability and extrudability of the gel formulation were assessed in accordance with the described protocol. To sum up, three sets of 1 g and 10 g of gel were used for spreadability and extrudability tests, respectively. In order to do spreadability efficiency study on the gel formulations, the measured quantity of the sample was deposited on one glass slide, and another glass slide was positioned over the gel, sandwiching the sample between the two glass slides(Khan et al. 2022). The samples were then compressed between the top and bottom glass slides with a 100 g weight to produce a consistent thin layer. The extra sample was taken out. Furthermore, after being fastened with a 20 g weight, only the upper glass slide should be simple to remove; the

second glass slide was firmly fastened to the platform with little to no harm(Srividya et al. 2022). Spreadability was measured as the amount of time needed to move the top glass 7.50 cm across the thin sheet on the bottom glass slide. In parallel, the extrudability of the generated gel compositions was estimated by measuring the quantity of gel that extruded from collapsible tubes. Nanogel and conventional gel, two distinct gel compositions, were weighed and placed into collapsible tubes. Extrudability (g cm−2) was then computed using the weight (g) required to extrude a 1 cm ribbon of the formulations from the collapsible tubes(Raja et al. 2021).

Viscosity

Using a Brookfield Rheometer, the viscosity was determined (Brookfield, USA). Topical nanogel was added to the sample container until it reached the designated mark. The spindle CCT-14 was connected to the Brookfield Rheometer. The spindle was dipped into a sample container that had already been loaded with topical nanogel. After that, a sample container was fastened to the device, and the viscosity of the topical nanogel was determined(Hassan and Hasary 2023).

Pre-clinical Evaluation of nanogel

Animal Treatment

Male Sprague-Dawley (SD) rats, aged five weeks and weighing between 160–210 g, were obtained from the University's animal house. They were housed in stainless steel cages at the Department of Pharmacology's animal house, maintaining ambient conditions of temperature (25°C), light, and relative humidity (55 to 60%)(Nascimento et al. 2024). The rats were fed a conventional rodent diet from M/s. Golden Feeds, Mehrauli, New Delhi, India, for the duration of the trials. Before the trial started, the animals spent more than seven days becoming acclimated to conventional laboratory settings, which included 22 ± 2 °C, 55 ± 10% humidity, and a 12-hour light/dark cycle. Before the experiment began, the animals were given free reign to eat and drink for a week as part of their acclimation phase. At the end of the trial, pentobarbitone (35 mg/kg body weight) was injected intraperitoneally to induce anaesthesia and make it easier to draw blood from retroorbital veins. The animals were observed every day for five days prior to the experiment, during which time their behaviour, clinical symptoms, illness, and death were recorded. All animals were permitted to breathe on their own during the procedure(Al-Hayder, Aledani, and Al-Mayyahi 2022).

Induction of osteoarthritis

Four sets of six SD rats each were created: sham, control, topical nanogel, and diclofenac. Monosodium iodoacetate (MIA) (Sigma, USA) was dissolved in 0.9% saline to create a solution with a concentration of 40 mg/mL. After being put to sleep with 2% isoflurane, the rats were given an intracapsular injection of the MIA solution (50 µL) via the infrapatellar ligament into the knee joint. This procedure was done under the published literature's guidelines for inducing experimental osteoarthritis (OA) in rats. The identical injection process was performed in a sham group, but 50 µL of regular saline solution was used instead(Ilyas et al. 2020).

Interventions

Four groups of rats were randomly assigned one week after OA induction: an untreated sham OA group, an active control group that received 0.4 g of diclofenac 1% gel daily for three weeks, and experimental groups that received topical 1% nano gel at standardized daily doses that were comparable to the active comparator. An inert vehicle gel weighing 1 g/kg was applied topically to the sham group(Al-Mukhtar, Deleme, and Khudhur 2023).

Study Outcome measurements

We assessed the anti-inflammatory efficacy across all animal groups at the end of the three-week treatment period. Serum levels of two inflammatory cytokines, interleukins and tumour necrosis factor-alpha (TNF-α), were measured as part of this evaluation. Joint mobility, motor function, and movement-induced discomfort were all assessed as part of the study(Šléglová 2023). Using the accelerating rotarod apparatus (Ugo Basile, Varese, Italy, Model 7750), this assessment was carried out once a week in compliance with the protocol

described by earlier research. In addition, we kept track of the animals' body weight for the whole trial(Brumat et al. 2022).

Progression of OA and Hind Paw Weight-Bearing `Distribution

All rats were allowed to roam around in their cages on days 0, 7, 14, and 21 after the test material was administered. Their gait patterns, including any indications of disruption, and the swelling in their knee joints were carefully evaluated. The arthritis index (AI) score was calculated by classifying the degree of swelling and limping into four categories: mild (1), moderate (2), severe (3), and no change (0) [233,234]. The same qualified assessor, who was not aware of the treatment assignments, performed the evaluations for the duration of the trial(Aso et al. 2022).

Following the onset of osteoarthritis (OA), an imbalance in the hind paws' capacity to support body weight was observed. Rats were carefully placed in a measuring chamber fitted with a capacitance metre tester (IITC Life Science, Woodland Hills, CA, USA) in order to measure changes in weight-bearing tolerance(Li et al. 2020).

Every hind limb's force was averaged during a ten-second period. Weight distribution of left hind paw = weight on left hind limb / (weight on right hind limb + weight on left hind limb) × 100 is the formula used to compute the percentage of weight distribution on the left hind paw(Hsieh et al. 2023).

Molecular biomarkers using Serum for OA Induced Model

To allow for clotting, blood samples were taken from the abdomen vein and kept undisturbed for 30 minutes. After that, the serum was removed by centrifugation for 10 minutes at 4000 rpm, and it was kept for further examination at -70 °C. The Premixed Multi-Analyte Kit from Thermofisher Scientific, USA, was used in combination with Invitrogen-Rat ELISA Kits to determine the amounts of IL-1β, IL-6, and TNF-α. Using a Luminex MAGPIX analyzer (Luminex Co., Austin, USA), the acquired data were examined following the guidelines supplied by the manufacturers for each multiplex test(Y. M. Lee et al. 2023).

Screening of anti-inflammatory activity of nanogel using paw edema

Our model of MIA-induced arthritis served as a useful tool for assessing the topical gel formulation's effectiveness. Following a week of acclimatisation in the animal housing facility, 24 rats were divided into four groups (n = 6) at random and placed into individual housing. Below is the breakdown of the groups: 0.2 cc of paraffin oil was injected into the right hind paw's sub-planter area every four days for a total of twelve days in Group I, which was assigned as the vehicle control(J. A. Lee et al. 2023). The arthritic control group was represented by Group II, the conventional test group by Group III, and the experimental group by Group IV. Every four days for a duration of twelve days, the sub-planter region of the right hind paw was injected subcutaneously with 0.2 ml of Complete Freund's Adjuvant, which is made up of powdered mycobacterium cells that have been heat-killed and suspended in liquid paraffin, into the remaining three groups (Groups II to IV). Using a digital scale and plethysmograph, data on body weight and rat paw volume were acquired before and after the research period on days 0, 5, 9, and 12. Treatment was started on day 13 with different formulations and maintained topically for the next two weeks. Days 17, 22, and 27 of the treatment periods were used to measure the body weight and rat paw volume of the test and control groups(Gharat, Basudkar, and Momin 2024).

Assessment of skin tolerance

The rats were divided into pairs, each consisting of four creatures. An animal hair clipper measuring 0.1 mm was used to cut the hair on their backs. After that, their skin was washed and shaved three- or four-times using cotton soaked in saline. Every animal was kept separately in a cage with unrestricted access to food and water. Topical nanogel was applied to one pair of animals, and conventional gel was applied to the other pair. For a duration of two weeks, each pair received the corresponding formulations at a dose of one gramme daily(Donaldson et al. 2020). Every day checks were performed to keep an eye out for any changes to the skin. Using cloth soaked in saline, any formula left on the skin was carefully cleansed at the conclusion of the

treatment session. A scoring system was used to assess the skin surface and look for indications of erythema or edoema. The values for erythema (0, no erythema; 1, slight; 2, well defined; 3, moderate; 4, scar formation) and edoema (0, no edoema; 1, slight; 2, well defined; 3, moderate; 4, severe) were incorporated in this system. At last, an analysis was conducted on the data gathered from these evaluations(Mendoza and Rodríguez 2022).

Statistical analysis

The data were subjected to statistical analysis utilizing the SPSS statistics program version 15.0 (SPSS, Chicago, IL, USA). The data was shown as means plus or minus standard deviation. One-way analysis of variance was used to statistically evaluate quantitative differences between values, and for numerous intergroup comparisons, Tukey or Dunnett post hoc tests were used. Two dependent groups were compared using paired sample t-tests. P-values less than 0.05 were regarded as statistically meaningful(Zemánková et al. 2023).

Results & Discussion

Determination of pH

pH was observed as 6.63 ± 0.34 (Table 1). The pH of topical nanogel should be in between 5.5 to 7.0 to avoid tendency of irritation when applied to skin. Therefore, the formulated nanogel possess desired pH and could be suitable for applying over skin.

Homogeneity

The uniformity of the topical nanogel formulation was examined following its filling into flint-colored glass containers. This assessment aimed to ensure homogeneity by checking for the presence of any aggregates. The prepared topical nanogel formulation demonstrated homogeneity, as no aggregates were detected.

Spread ability and extrudability

Spreadability was used to evaluate the topical nanogel compositions' ability to spread. Important factors affecting the even dispersion and patient compliance of gel compositions include spreadability and extrudability. The nanogel exhibited a spreadability of 65.67 ± 3.77 gm.cm/s and an extrudability of 103.16 ± 3.83 gm/cm2 (Table 1). Therefore, the prepared topical nanogel formulation showed good consistency and spread ability.

Viscosity

The viscosity of topical nanogel formulation was found as 108.6 ± 5.43 cp (Table 1). Viscosity is essential for the effective distribution of gels, emulsions, and solutions as well as their stable manufacture. The study reveals that, the prepared topical nanogel formulation possess desired viscosity with consistency.

Table 1: Data reflects the nanogel evaluation and its average values.

Parameters	Nanogel			
	I	II	III	Average ± SD
Colour	Creamy	Creamy	Creamy	Creamy
Appearance	Translucent	Translucent	Translucent	Translucent
Homogeneity	Good	Good	Good	Good
pH	6.87	6.24	6.77	6.63 ± 0.34
Spreadability (gm.cm/sec)	65.52	69.51	61.97	65.67 ± 3.77
Extrudability	107.41	102.11	99.96	103.16 ± 3.83

(gm/cm^2)				
Viscosity (cp)	102.4	110.9	112.5	108.6 ± 5.43

Body weight measurements

The study monitored the rat body weight in the experimental groups both prior to and following the initiation of the treatment protocol. This information is detailed in Table 2. It was observed that the test groups experienced a decrease in body weight after the onset of the disease. Conversely, the normal control group exhibited weight gain after the commencement of treatment. Notably, the arthritic control group displayed a reduction in body weight. This outcome could potentially be linked to abnormal metabolic processes.

Table 2: Effect of treatment on body weight of animals

Groups	Body weight (g)					Weight gain (g)
	Initial	12 days	17th day	22nd day	27th day	
Normal Control	147.1± 0.55	159.4± 1.33	166.5± 0.75	171.3± 1.22	182.2± 0.36	35.1± 0.62
Arthritic Control	161.4± 0.47	159.3± 0.25	151.7± 0.66	148.1± 0.35	141.4± 0.55	-20.1± 0.22
1% diclofenac gel	160.4± 0.25	161.7± 0.55	165.8± 0.29	167.5± 0.16	168.6± 0.12	8.2± 0.56
Novel Nanogel formulation	161.5± 0.47	164.7 ± 0.32	169.4 ± 0.40	170.1 ± 0.21	171.1 ± 0.15	9.6± 0.32

Evaluation of joint pain, mobility, and motor coordination

Rats utilising the rotarod apparatus showed a much shorter rotation duration when osteoarthritis (OA) was induced by intra-articular injection of MIA (Table 3). It is most likely due to actively inflamed, swollen, stiff, and painful joints since this reduction shows a deterioration in joint motor function, mobility, and the capacity to maintain balance on the revolving spindle. Comparing the newly produced nanogel formulation group to the untreated OA group, the latter group's duration on the rotarod device in seconds demonstrated a significant decrease in mobility throughout the course of the full trial period (Table 3). The osteoarthritis group, on the other hand, continuously demonstrated a significantly lower rotarod delay than the sham control group during the course of the 4-week investigation. Compared to the osteoarthritis control group, rats treated with diclofenac gel showed a notable increase in rotarod latency after three weeks of administration, whereas the novel nanogel formulation demonstrated a significant increase in the amount of time rats could stay on the rotarod after two weeks of treatment (Table 3). This implies that in these therapy groups, there was an improvement in joint mobility, motor function, and decreased pain related to movement (better analgesia) in our arthritic model. Furthermore, only three weeks into therapy did the diclofenac gel-treated actively compared group exhibit a statistically significant extension in rotation length.

Table 3: Effect of novel nanogel on motor activity. Data represent the mean ± SEM of eight animals.

	Rotarod latency (s)

Groups	Baseline	1st week post-treatment	2nd week post-treatment	3rd week post-treatment
Sham	260.9[b] ± 4.57	251.4[b] ± 10.09	236.2[b] ± 11.88	256.9[b] ± 6.82
Osteoarthritis control	186.4[a] ± 4.09	163.5[a] ± 10.5	151.2[a] ± 10.02	148.1[a] ± 10.10
1% diclofenac gel	190.9[a] ± 4.25	208.6 ± 5.10	229.2 ± 2.67	242.7[b] ± 4.14
Novel Nanogel formulation	194.6[a] ± 4.10	193.5 ± 6.25	198.3[a] ± 7.16	221.2 ± 6.09

[a]$p \leq 0.05$ indicates significant differences as compared with the sham control group; [b]$p \leq 0.05$ versus osteoarthritis group

Impact of a Novel Nanogel on the Weight-Bearing Distribution of the Hind Paw in Rats with MIA-Induced Osteoarthritis for 21 Days

Using an in-capacitance tester, we measured the ratio of weight distribution between the left (MIA-injected) and right (healthy) limbs on days 0, 7, 14, and 21 in order to determine the evolution of OA in the hind paw. The weight distribution ratio of the MIA-treated group was significantly lower than that of the control group on day 7, and this difference persisted until day 21 ($p < 0.01$) (Table 4).

On the other hand, the results showed that the recently developed nanogel greatly reduced discomfort and improved the ability to support weight.

Table 4: MIA-induced osteoarthritis in rats, the impact of the innovative nanogel formulation on hind paw weight-bearing distribution was evaluated over a 21-day period

Treatment	Weight Bearing Distribution (%)			
	Day 0	Day 7	Day 14	Day 21
Sham	51.51 ± 0.95	50.52 ± 0.50	53.25 ± 0.82	49.22 ± 0.55
Osteoarthritis control	35.25 ± 1.56 ##	30.25 ± 2.35 ##	33.45 ± 1.31 ##	35.66 ± 1.02 ##
1% diclofenac gel	30.55 ± 3.65	36.98 ± 2.43	39.55 ± 1.29	43.79 ± 2.02 *
Novel Nanogel formulation	31.46 ± 2.27	37.05 ± 2.55 *	40.25 ± 1.50 *	42.88 ± 0.96 *

The data are presented as mean ± SEM (n = 6/group). * $p < 0.05$, ** $p < 0.01$, compared to the MIA-induced control group; ## $p < 0.01$, compared to the non-MIA-induced control group.

Activity of nanogel formulation gel on Arthritis Index (AI) for 21 Days in MIA-Induced Osteoarthritis

We observed all the animals once a week in order to look for general signs of OA, such as oedema and limping (Table 5). Compared to the other groups, the MIA-treated group had a higher arthritis index (AI) score, which includes both swelling and limping. The MIA-treated group's AI score steadily dropped over time (see Table 2). When compared to the MIA-treated group, rats treated with 1% diclofenac gel showed noticeably worse AI scores starting on day 14. Furthermore, the results showed a significant decline in AI scores after day 21, with the values eventually approaching those of the positive control, diclofenac. We therefore verified that the topical administration of the new nanogel formulation significantly reduced the higher AI scores associated with OA.

Table 5: Effects of novel nanogel formulation on arthritis index (AI)

Treatment	Arthritis Index (AI)

	Day 0	Day 7	Day 14	Day 21
Sham	0.00	0.00	0.00	0.00
Osteoarthritis control	2.05 ± 0.31 ##	2.01 ± 0.15 ##	1.65 ± 0.04 ##	1.41 ± 0.21 ##
1% diclofenac gel	1.95 ± 0.19	1.59± 0.33	1.06 ± 0.07 **	0.69 ± 0.25 **
Novel Nanogel formulation	2.02 ± 0.15	1.68 ± 0.14	1.20 ± 0.22 **	0.92 ± 0.10 **

The presented data are expressed as mean ± SEM (n = 8/group). ** $p < 0.01$, indicating a significant difference compared to the MIA-induced control group; ## $p < 0.01$, indicating a significant difference compared to the non-MIA-induced control group

Role on Inflammatory Cytokines in MIA-Induced Rat Model

After serum was extracted from blood samples in every experimental group, the levels of inflammatory cytokines in the serum were measured. Compared to the control group, rats treated topically with the recently created nanogel showed a substantial decrease in IL-1β, IL-6, and TNF-α concentrations, suggesting a dose-dependent impact. Interestingly, the nanogel showed a notable decrease in cytokine levels that was on par with the positive control group
that received 1% diclofenac gel treatment (Figure 1.).

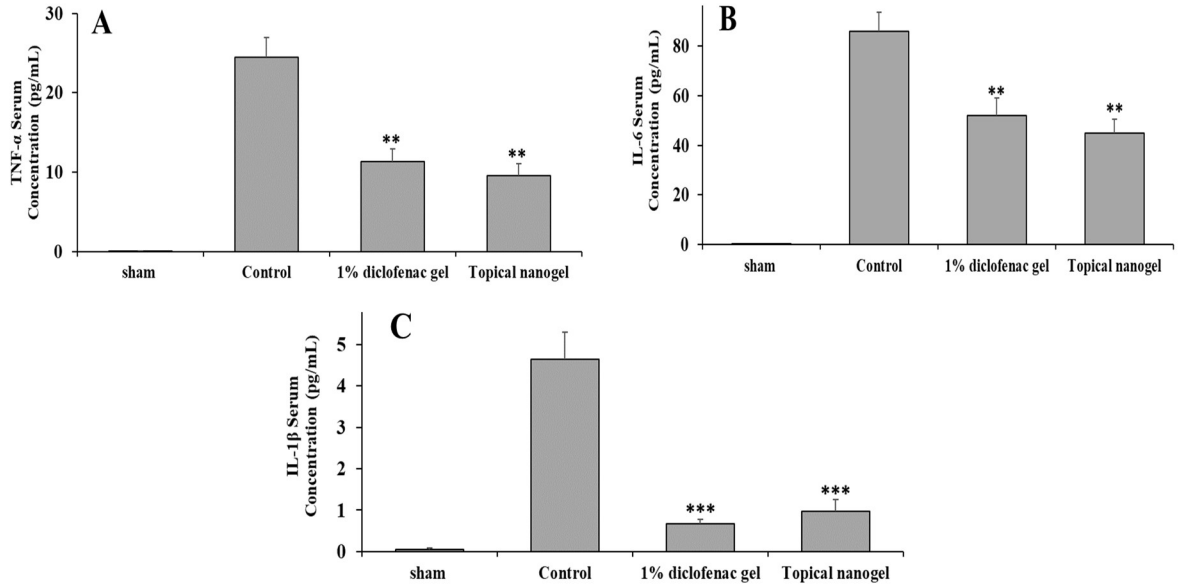

Figure 1. Effect of novel formulated nanogel on the inhibitory effects on serum inflammatory cytokine levels in monosodium iodoacetate (MIA) rats. All the experimental rats were topically administered the nanogel for 21 days, ** $p < 0.01$ vs. control, *** $p < 0.001$ vs. control by one-way ANOVA, Dunnett's test.

***In Vivo* Skin Safety Study**

For both the nanogel and the traditional gel, we performed in vivo skin safety evaluations, paying particular attention to possible skin irritation at the application site. Both formulations scored 0 after two weeks, meaning there were no symptoms of discomfort. Interestingly, there was no sign of erythema or edoema development. These findings demonstrate the improved safety profile of the optimised nanogel as a topical medication delivery method. This implies that when it comes to skin safety, the nanogel is a better option than the traditional gel.

Paw volume measurement

Rat paw volumes were measured on the 17th, 22nd, and 27th days after the topical administration of nanogel from the 13th to the 27th day. The changes in paw volume were measured using a plethysmometer. Rat paw volume increased significantly in the arthritic control group but decreased significantly in the test group

following the start of the treatment regimen. Table 6 displays the information assessing anti-arthritic activity by measuring paw volume. Paw volume rose from 0.24 ± 0.11 to 0.83 ± 0.08 (245%) in the arthritic control group. The paw volume for the nanogel group dropped from 0.49 ± 0.04 on day 12 after induction to 0.26 ± 0.09 on day 27. In contrast, the positive control diclofenac gel exhibited a significant reduction in paw volume, measuring 0.47 ± 0.06 on day 12 and 0.28 ± 0.05 on day 27, respectively. These results affirm the effectiveness of the nanogel formulation in reducing paw volume to levels similar to diclofenac gel, indicating its comparable efficacy. This outcome can be attributed to the novel nanogel formulations that significantly penetrated the skin compared to the conventional drug gel.

Table 6: Anti-arthritic activity of novel nanogel.

Groups	Paw volume (ml)				
	Before Treatment	After Treatment			
	Initial	After 12 days	17th day	22nd day	27th day
Sham	0.21 ± 0.02	0.21 ± 0.01	0.21 ± 0.04	0.21 ± 0.05	0.21 ± 0.03
Osteoarthritis control	0.24 ± 0.11	0.46 ± 0.02	0.57 ± 0.04	0.71 ± 0.03	0.83 ± 0.08
1% diclofenac gel	0.21 ± 0.03	0.47 ± 0.06	0.41 ± 0.07	0.36 ± 0.05	0.28 ± 0.05
Novel Nanogel formulation	0.22 ± 0.04	0.49 ± 0.04	0.42 ± 0.11	0.32 ± 0.01	0.26 ± 0.09

Conclusions

In conclusion, the comprehensive evaluation of our study provides potential therapeutic benefits of the newly developed nanogel formulation in the context of MIA-induced osteoarthritis in rats. The key findings and implications can be summarized as follows: The experimental groups exhibited distinct patterns of body weight changes. Notably, the arthritic control group showed a decrease in body weight, possibly linked to abnormal metabolic processes during arthritic conditions, including insulin resistance. In contrast, the normal control group demonstrated weight gain after treatment initiation, highlighting the significance of our treatment interventions. The induction of osteoarthritis led to a decline in joint motor function, mobility, and balance, as evidenced by reduced rotarod performance. However, the novel nanogel formulation consistently improved joint mobility and motor coordination, with significant enhancements observed after just 2 weeks of treatment. This improvement was comparable to diclofenac gel, suggesting the efficacy of our nanogel in alleviating pain and enhancing mobility associated with osteoarthritis. The data showed that the MIA-induced group exhibited a lower weight distribution ratio compared to the normal control group, indicating reduced weight-bearing capacity due to osteoarthritis. However, the newly formulated nanogel significantly alleviated pain and improved weight-bearing abilities. The arthritis index scores, encompassing swelling and limping, were notably higher in the MIA-induced group initially. The nanogel formulation consistently reduced AI scores, with significant improvements observed after 14 days, comparable to diclofenac gel. This suggests that our nanogel effectively mitigated the symptoms associated with osteoarthritis. Cytokines level such as IL-1β, IL-6, and TNF-α were significantly reduced in rats treated with the nanogel, demonstrating a dose-dependent effect. These reductions were comparable to the positive control group treated with diclofenac gel, indicating the anti-inflammatory potential of the nanogel. In-vivo skin safety assessments revealed that both the nanogel and conventional gel formulations were well-tolerated, with no signs of irritation, edema, or erythema. This highlights the superior safety profile of the nanogel for topical application. The nanogel formulation demonstrated a significant reduction in paw volume, similar to the effect observed with diclofenac gel. This indicates the nanogel's effectiveness in reducing inflammation and swelling associated with arthritis, potentially due to its superior skin penetration properties.

In summary, our study provides compelling evidence that the novel nanogel formulation offers a promising therapeutic approach for the management of osteoarthritis in rats. It effectively improved joint mobility, reduced

pain, mitigated inflammation, and demonstrated excellent skin safety. These findings suggest that the nanogel formulation could be a valuable candidate for further development as a topical treatment option for osteoarthritis in humans, potentially offering advantages over conventional gel formulations. Further research and clinical trials are warranted to explore its full therapeutic potential and safety in human subjects.

Acknowledgement
The authors would like to express their sincere gratitude to our Institution for providing the necessary resources and support for this research. Special thanks to the research team and laboratory staff for their invaluable assistance. We also appreciate the contributions of all collaborators who made this study possible.

Conflict of Interest
None

REFERENCES

1. Afshar, Maryam, Leila Dolatyari, Payam Soheili-Azad, Mir Saeid Seyyed Dorraji, and Mohammad Reza Yaftian. 2024. "Unmodified and RGO-Modified Zn/Al Layered Double Hydroxides; Nanoadsorbents Employed for the Solid Phase Extraction/HPLC Determination of Naproxen." *Journal of Dispersion Science and Technology*. doi: 10.1080/01932691.2023.2247061.
2. Ahmad, Rahaf M., Yaser E. Greish, Hesham F. El-Maghraby, Loay Lubbad, Yahia Makableh, and Fayez T. Hammad. 2022. "Preparation and Characterization of Blank and Nerolidol-Loaded Chitosan–Alginate Nanoparticles." *Nanomaterials*. doi: 10.3390/nano12071183.
3. Al-Hayder, Manal N., Tamadir H. W. Aledani, and Rawaa S. Al-Mayyahi. 2022. "Amelioration of the Hepatotoxic Effects of Nonsteroidal Drugs Using Vitamin C and Determination of Their Relationship with the Lipid Profile." *Journal of Taibah University Medical Sciences*. doi: 10.1016/j.jtumed.2021.11.003.
4. Al-Mukhtar, Yusra Hameed, Zaid Hazim Deleme, and Ahmed Salih Khudhur. 2023. "Evaluating the Efficacy of Etoricoxib in Reducing Post-Operative Pain Associated with Minor Oral Surgery. A Randomized Clinical Trial." *Brazilian Dental Science*. doi: 10.4322/BDS.2023.E3854.
5. Aljubailah, Abeer, Saad M. S. Alqahtani, Tahani Saad Al-Garni, Waseem Sharaf Saeed, Abdelhabib Semlali, and Taieb Aouak. 2022. "Naproxen-Loaded Poly(2-Hydroxyalkyl Methacrylates): Preparation and Drug Release Dynamics." *Polymers*. doi: 10.3390/polym14030450.
6. Allen, K. D., L. M. Thoma, and Y. M. Golightly. 2022. "Epidemiology of Osteoarthritis." *Osteoarthritis and Cartilage*. doi: 10.1016/j.joca.2021.04.020.
7. Arslan, Yasin, Fatma Tomul, Neslihan Kaya Kınaytürk, Nguyen Thanh Dong, Diğdem Trak, Burcu Kabak, and Hai Nguyen Tran. 2024. "Important Role of Pore-Filling Mechanism in Separating Naproxen from Water by Micro-Mesoporous Carbonaceous Material." *Water Environment Research*. doi: 10.1002/wer.10966.
8. Aso, K., D. A. Walsh, H. Wada, M. Izumi, H. Tomitori, K. Fujii, and M. Ikeuchi. 2022. "Time Course and Localization of Nerve Growth Factor Expression and Sensory Nerve Growth during Progression of Knee Osteoarthritis in Rats." *Osteoarthritis and Cartilage*. doi: 10.1016/j.joca.2022.07.003.
9. Ayorindea, J. O., P. C. Agbolabori, and M. A. Odeniyia. 2023. "Preparation, Characterization and Release Studies of Naproxen-Loaded Microspheres from Natural Gums." *Nigerian Journal of Pharmaceutical Research*. doi: 10.4314/njpr.v18i2.8.
10. Bella Triana, and Anan Suparman. 2022. "Kajian Pengembangan Etosom Sebagai Pembawa Agen NSAID Topikal." *Jurnal Riset Farmasi*. doi: 10.29313/jrf.v2i2.1274.
11. Biswasroy, Prativa, Deepak Pradhan, Dilip Kumar Pradhan, Goutam Ghosh, and Goutam Rath. 2024. "Development of Betulin-Loaded Nanostructured Lipid Carriers for the Management of Imiquimod-Induced Psoriasis." *AAPS PharmSciTech*. doi: 10.1208/s12249-024-02774-1.
12. Brumat, Peter, Ožbej Kunšič, Samo Novak, Urban Slokar, Janez Pšenica, Matevž Topolovec, Rene

Mihalič, and Rihard Trebše. 2022. “The Surgical Treatment of Osteoarthritis.” *Life*.
13. Campos, Mariana G. M., Laísa B. Maia, Rodrigo O. Mascarenhas, Bianca M. Lourenço, Nicholas Henschke, and Vinicius C. Oliveira. 2024. “Effectiveness of Non-Invasive Therapies on Pain, Maximum Grip Strength, Disability, and Quality of Life for Lateral Elbow Tendinopathy: A Systematic Review and Meta-Analysis.” *Brazilian Journal of Physical Therapy*.
14. Chettupalli, Ananda Kumar, Srivani Ajmera, Padmanabha Rao Amarachinta, Ram Mohan Manda, and Rajendra Kumar Jadi. 2023. “Quality by Design Approach for Preparation, Characterization, and Statistical Optimization of Naproxen Sodium-Loaded Ethosomes via Transdermal Route.” *Current Bioactive Compounds*. doi: 10.2174/1573407219666230606142116.
15. Ciurba, Adriana, Aurelia Gabriela Popescu, Robert Alexandru Vlad, Emőke Rédai, Nicoleta Todoran, Cornelia Titiana Cotoi, Magdalena Bîrsan, and Paula Antonoaea. 2023. “DEVELOPMENT AND EVALUATION OF BIGELS CONTAINING NAPROXEN SODIUM FOR TOPICAL ADMINISTRATION.” *Farmacia*. doi: 10.31925/farmacia.2023.4.13.
16. Dell’Isola, Andrea, Aleksandra Turkiewicz, Weiya Zhang, Ali Kiadaliri, Sita Bierma-Zeinstra, Jos Runhaar, Daniel Prieto-Alhambra, and Martin Englund. 2022. “Does Osteoarthritis Modify the Association between NSAID Use and Risk of Comorbidities and Adverse Events?” *Osteoarthritis and Cartilage Open*. doi: 10.1016/j.ocarto.2022.100253.
17. Fatih Dilekoglu, Mehmet, and Mazlum Yapici. 2023. “Adsorption of Naproxen Pharmaceutical Micropollutant from Aqueous Solutions on Superior Activated Carbon Synthesized from Sheep Manure: Kinetics, Thermodynamics, and Mechanism.” *Journal of Molecular Liquids*. doi: 10.1016/j.molliq.2023.121839.
18. Freitas, E. D., P. C. P. Rosa, M. G. C. Silva, and M. G. A. Vieira. 2021. “Application of Experimental Design to Evaluate the Incorporation of Naproxen into Sericin/Alginate Particles Prepared by Ionic Gelation Technique.” *Chemical Engineering Science*. doi: 10.1016/j.ces.2020.116101.
19. Gharat, Sankalp, Vivek Basudkar, and Munira Momin. 2024. “In-Vitro and in-Vivo Evaluation of the Developed Curcumin-Cyclosporine-Loaded Nanoemulgel for the Management of Rheumatoid Arthritis.” *Immunological Investigations*. doi: 10.1080/08820139.2024.2301997.
20. Hassan, Dastan Salim, and Hemin Jumaa Hasary. 2023. “The Impact of Viscosity on the Dissolution of Naproxen Immediate-Release Tablets.” *Journal of Taibah University Medical Sciences*. doi: 10.1016/j.jtumed.2022.12.009.
21. Heidari-Beni, Motahar, Amir R. Moravejolahkami, Pegah Gorgian, Gholamreza Askari, Mohammad J. Tarrahi, and Nimah Bahreini-Esfahani. 2020. “Herbal Formulation ‘Turmeric Extract, Black Pepper, and Ginger’ versus Naproxen for Chronic Knee Osteoarthritis: A Randomized, Double-Blind, Controlled Clinical Trial.” *Phytotherapy Research*. doi: 10.1002/ptr.6671.
22. Hinman, Rana S., Michelle Hall, Sarah Comensoli, and Kim L. Bennell. 2023. “Exercise & Sports Science Australia (ESSA) Updated Position Statement on Exercise and Physical Activity for People with Hip/Knee Osteoarthritis.” *Journal of Science and Medicine in Sport*. doi: 10.1016/j.jsams.2022.11.003.
23. Hsieh, Cheng Yang, Ching Chiung Wang, Lemmuel L. Tayo, Shun Xin Deng, Po Wei Tsai, and Chia Jung Lee. 2023. “In Vitro and in Vivo Anti-Osteoarthritis Effects of Tradition Chinese Prescription Ji-Ming-San.” *Journal of Ethnopharmacology*. doi: 10.1016/j.jep.2022.116084.
24. Ilyas, Sajida, Kashif Jilani, Muhammad Sikandar, Saba Siddiq, Muhammad Riaz, Ayesha Naveed, Ismat Bibi, Haq Nawaz, Muhammad Irfan, and Asma Asghar. 2020. “Stimulation of Erythrocyte Membrane Blebbing by Naproxen Sodium.” *Dose-Response*. doi: 10.1177/1559325819899259.
25. Inagaki, Junko, Airi Nakano, Omer Faruk Hatipoglu, Yuka Ooka, Yurina Tani, Akane Miki, Kentaro Ikemura, Gabriel Opoku, Ryosuke Ando, Shintaro Kodama, Takashi Ohtsuki, Hirosuke Yamaji, Shusei Yamamoto, Eri Katsuyama, Shogo Watanabe, and Satoshi Hirohata. 2022. “Potential of a Novel Chemical Compound Targeting Matrix Metalloprotease-13 for Early Osteoarthritis: An In Vitro Study.” *International Journal of Molecular Sciences*. doi: 10.3390/ijms23052681.
26. Ivković, Branka, Milkica Crevar, Anka Cvetanović, Katarina Ubavkić, and Bojan Marković. 2023. “Development and Validation of RP-HPLC Method for Quantification of Trace Levels of Topical

Corticosteroids in Ambiphilic Cream." *Acta Chromatographica*. doi: 10.1556/1326.2021.00998.
27. Jadhav, Vrushali R., and Kiran B. Erande. 2023. "Formulation and Evaluation of Biopolymer Incorporated Nanogel of Nabumetone." *Biosciences Biotechnology Research Asia*. doi: 10.13005/bbra/3187.
28. Jalil, Reza-Ul, Jakir Ahmed Chowdhury, and Fuad M. Laman. 2023. "Design and In-Vitro Evaluation of Compressed Kollidon® SR Based Naproxen Sodium Microcapsule: Effect of Talc." *Journal of Drug Delivery and Therapeutics*. doi: 10.22270/jddt.v13i3.5752.
29. Jin, Suxing, Nafees Muhammad, Yuewen Sun, Yehong Tan, Hao Yuan, Dongfan Song, Zijian Guo, and Xiaoyong Wang. 2020. "Multispecific Platinum(IV) Complex Deters Breast Cancer via Interposing Inflammation and Immunosuppression as an Inhibitor of COX-2 and PD-L1." *Angewandte Chemie - International Edition*. doi: 10.1002/anie.202011273.
30. Joshi, Medhavi V, and Pratik Phansopkar. 2022. "Superior Replacement of Medicinal Gel With Ayurvedic Nanogel as a Coupling Medium for Electrotherapeutic Treatment of Osteoarthritis: A Review Article." *Cureus*. doi: 10.7759/cureus.28658.
31. Karateev, Andrey E., Aleksander M. Lila, and Lyudmila I. Alekseeva. 2021. "Use of Tanezumab for Chronic Pain Treatment." *Nauchno-Prakticheskaya Revmatologiya*. doi: 10.47360/1995-4484-2021-192-200.
32. Khan, Barkat Ali, Sajeel Ahmad, Muhammad Khalid Khan, Khaled M. Hosny, Deena M. Bukhary, Haroon Iqbal, Samar S. Murshid, Abdulrahman A. Halwani, Mohammed Alissa, and Farid Menaa. 2022. "Fabrication and Characterizations of Pharmaceutical Emulgel Co-Loaded with Naproxen-Eugenol for Improved Analgesic and Anti-Inflammatory Effects." *Gels*. doi: 10.3390/gels8100608.
33. Kianersi, Sogol, Atefeh Solouk, Saeed Saber-Samandari, Saeed Heidari Keshel, and Pooria Pasbakhsh. 2021. "Alginate Nanoparticles as Ocular Drug Delivery Carriers." *Journal of Drug Delivery Science and Technology*. doi: 10.1016/j.jddst.2021.102889.
34. Kolding, L., I. Cem Özok, T. Henriksen, and L. H. Pedersen. 2023. "EP08.18: No Differences in Neonatal Outcomes between Two Pharmacokinetic Different Formulations of Betamethasone." *Ultrasound in Obstetrics & Gynecology*. doi: 10.1002/uog.26745.
35. Lee, Jin A., Trung Huy Ngo, Mi Rae Shin, Jeong Won Choi, Hyukjae Choi, Joo Won Nam, and Seong Soo Roh. 2023. "Efficacy of Veronica Incana for Treating Osteoarthritis Induced by Monosodium Iodoacetate in Rats." *Journal of Medicinal Food*. doi: 10.1089/jmf.2023.K.0001.
36. Lee, Yun Mi, Misun Kim, Heung Joo Yuk, Seung Hyung Kim, and Dong Seon Kim. 2023. "Siraitia Grosvenorii Residual Extract Inhibits Inflammation in RAW264.7 Macrophages and Attenuates Osteoarthritis Progression in a Rat Model." *Nutrients*. doi: 10.3390/nu15061417.
37. Li, Hui, Xiang Ding, Robert Terkeltaub, Hang Lin, Yuqing Zhang, Bin Zhou, Ke He, Kun Li, Zhichen Liu, Jie Wei, Yuanheng Yang, Hui Xie, Chao Zeng, and Guanghua Lei. 2020. "Exploration of Metformin as Novel Therapy for Osteoarthritis: Preventing Cartilage Degeneration and Reducing Pain Behavior." *Arthritis Research and Therapy*. doi: 10.1186/s13075-020-2129-y.
38. Li, Shangyong, Hui Zhang, Kaiwei Chen, Mengfei Jin, Son Hai Vu, Samil Jung, Ningning He, Zhou Zheng, and Myeong Sok Lee. 2022. "Application of Chitosan/Alginate Nanoparticle in Oral Drug Delivery Systems: Prospects and Challenges." *Drug Delivery*. doi: 10.1080/10717544.2022.2058646.
39. Ma, Yandong, Haiyuan Yang, Xiaoqing Zong, Jinpei Wu, Xin Ji, Wen Liu, Pengfei Yuan, Xinjie Chen, Caiqi Yang, Xiaodi Li, Yuanfeng Chen, Wei Xue, and Jian Dai. 2021. "Artificial M2 Macrophages for Disease-Modifying Osteoarthritis Therapeutics." *Biomaterials*. doi: 10.1016/j.biomaterials.2021.120865.
40. Mashoofnia, Anita, Zahra Mohamadnia, and Mohsen Kompany-Zareh. 2021. "Application of Multivariate and Spectroscopic Techniques for Investigation of the Interactions between Polyelectrolyte Layers in Layer-by-Layer Assembled PH-Sensitive Nanocapsules." *Macromolecular Chemistry and Physics*. doi: 10.1002/macp.202100107.
41. Medeiros, R. S., A. P. G. Ferreira, and E. T. G. Cavalheiro. 2023. "Chitosan and Naproxen Salts: Preparation and Characterization." *Journal of Thermal Analysis and Calorimetry*. doi: 10.1007/s10973-022-11626-8.

42. Medeiros, Ricardo S., Ana P. G. Ferreira, Tiago Venâncio, and Éder T. G. Cavalheiro. 2022. "Preparation, Characterization and Study of the Dissociation of Naproxen from Its Chitosan Salt." *Molecules*. doi: 10.3390/molecules27185801.
43. Mendoza, M., and O. Rodríguez. 2022. "COMPARACIÓN DE PARÁMETROS FÍSICO-QUÍMICOS DE COMPRIMIDOS DE CARVEDILOL DE 25MG GENÉRICO FRENTE AL MEDICAMENTO INNOVADOR." *Molecules*.
44. Mirocki, Artur, Mattia Lopresti, Luca Palin, Eleonora Conterosito, Artur Sikorski, and Marco Milanesio. 2022. "Exploring the Molecular Landscape of Multicomponent Crystals Formed by Naproxen Drug and Acridines." *CrystEngComm*. doi: 10.1039/d2ce00890d.
45. Mohamed, Magdy Ibrahim, Mohamed Aly Kassem, Rawia Mohamed Khalil, Mostafa Mohamed Younis, Asmaa Badawy Darwish, Abeer Salama, and Marwa Anwar Wagdi. 2021. "Enhancement of the Anti-Inflammatory Efficacy of Betamethasone Valerate via Niosomal Encapsulation." *Biointerface Research in Applied Chemistry*. doi: 10.33263/BRIAC116.1464014660.
46. Munir, Mehtab, Ayesha Khan, Tauseef Sayyar, Maria Mufti, Iqra Siddiqui, and Sara Tariq Abbasi. 2023. "Comparison Of Naproxen And Diacerein In The Treatment Of Knee Joint Osteoarthritis." *Journal of Rawalpindi Medical College*. doi: 10.37939/jrmc.v27i3.2034.
47. Nascimento, Bernardo Camara, Camila Stefane Ferreira, Stella Pollyanne Oliveira, Luiza Aparecida Ansaloni Chagas Pereira, Guilherme Antonio Lopes, Júlia Meireles Nogueira, Rayan Silva Paula, Erika Cristina Jorge, and Paulo Henrique Almeida Campos-Junior. 2024. "Naproxen Administration Affects Murine Late Folliculogenesis, Reduces Granulosa Cell Proliferation and the Number of Ovulated Oocytes." *Reproductive Toxicology*. doi: 10.1016/j.reprotox.2023.108527.
48. Nupur, Monia Akter, Mst Mahfuza Rahman, Khurshida Akter, Khadiza Binte Hanif, Jinat Fatema Sharna, Md Shahin Sarker, and Mir Imam Ibne Wahed. 2023. "Preparation and Characterization of Naproxen Solid Dispersion Using Different Hydrophilic Carriers and In-Vivo Evaluation of Its Analgesic Activity in Mice." *Heliyon*. doi: 10.1016/j.heliyon.2023.e15432.
49. Oteo Álvaro, A. 2021. "Ethiopathogenic Mechanism of Osteoarthritis." *Revista de La Sociedad Espanola Del Dolor*. doi: 10.20986/resed.2021.3851/2020.
50. Paget, Liam D. A., Gustaaf Reurink, Robert Jan de Vos, Adam Weir, Maarten H. Moen, Sita M. A. Bierma-Zeinstra, Sjoerd A. S. Stufkens, Rover Krips, Mario Maas, Duncan E. Meuffels, Gino M. M. J. Kerkhoffs, Johannes L. Tol, and Peter A. Nolte. 2023. "Platelet-Rich Plasma Injections for the Treatment of Ankle Osteoarthritis." *American Journal of Sports Medicine*. doi: 10.1177/03635465231182438.
51. Pan, Jun, Youzhi Cai, Chi Zhang, and Sanzhong Xu. 2023. "Intra-Articular Delivery of Geraniol Encapsulated by PH/Redox-Responsive Nanogel Ameliorates Osteoarthritis by Regulating Oxidative Stress and Inflammation." *Journal of Molecular Histology*. doi: 10.1007/s10735-023-10163-4.
52. Pergolizzi, J., G. Varrassi, P. Magnusson, J. A. L. Quang, R. Taylor, C. Wollmuth, F. Breve, K. Mitchell, M. Chopra, and P. J. Christo. 2020. "COVID-19 and NSAIDs: Knowns and Unknowns." *Postgraduate Medicine*.
53. Quddus, Farah, Afzal Shah, Jan Nisar, Muhammad Abid Zia, and Shamsa Munir. 2023. "Neem Plant Extract-Assisted Synthesis of CeO2 Nanoparticles for Photocatalytic Degradation of Piroxicam and Naproxen." *RSC Advances*. doi: 10.1039/d3ra04185a.
54. Raja, Mettupalayam Annadurai, Saranya Rajendran, Chamundeswari Kandasamy, Ganesh Kumar Gudas, and Kola Venu. 2021. "Formulation and Ex-Vivo Evaluation of Naproxen Emulgel by Skin Irritation Test." *Latin American Journal of Pharmacy*.
55. Ramos-Inza, Sandra, Cristina Morán-Serradilla, Leire Gaviria-Soteras, Arun K. Sharma, Daniel Plano, Carmen Sanmartín, and María Font. 2024. "Formulation Studies with Cyclodextrins for Novel Selenium NSAID Derivatives." *International Journal of Molecular Sciences*. doi: 10.3390/ijms25031532.
56. Ramos, Paweł, Barbara Klaudia Raczak, Daniele Silvestri, and Stanisław Wacławek. 2023. "Application of TGA/c-DTA for Distinguishing between Two Forms of Naproxen in Pharmaceutical Preparations." *Pharmaceutics*. doi: 10.3390/pharmaceutics15061689.
57. Rastegar Ramsheh, Zohreh Sadat, Zahra Mohtashami, Neda Kargar, Hamid Akbari Javar, Morteza Rafiee

Tehrani, and Farid Abedin Dorkoosh. 2021. "Design and In Vitro Evaluation of a Slow-Release Intraocular Implant of Betamethasone." *AAPS PharmSciTech*. doi: 10.1208/s12249-021-02048-0.
58. Reddyy, P. Srikanth, V. Alagarsamy, P. Subhash Chandra Bose, V. Sruthi, and D. Saritha. 2024. "Formulation and Evaluation of Naproxen Sodium Transdermal Patches Using Natural Polymer." *International Journal of Medical and Biomedical Studies*. doi: 10.32553/ijmbs.v8i1.2765.
59. Riccio, Bruno Vincenzo Fiod, Ana Beatriz Klosowski, Eduardo Prestes, Taynara Barbosa de Sousa, Laís Caroline de Assunção Morais, Bruna Mikulis Lemes, Flávio Luís Beltrame, Patrícia Mazureki Campos, and Priscileila Colerato Ferrari. 2021. "Chitosan/Nanocellulose-Based Bionanocomposite Films for Controlled Betamethasone and Silver Sulfadiazine Delivery." *Journal of Applied Polymer Science*. doi: 10.1002/app.50468.
60. Rojek, Barbara, Maria Gazda, and Alina Plenis. 2023. "FTIR, Raman Spectroscopy and HT-XRD in Compatibility Study between Naproxen and Excipients." *Spectrochimica Acta - Part A: Molecular and Biomolecular Spectroscopy*. doi: 10.1016/j.saa.2023.123048.
61. Sakib, Sakib, Vivek Verma, and Mojahid Ul Islam. 2022. "Formulation and Characterization of Topical Microemulsion Loaded with Naproxen." *International Journal of Health Sciences*. doi: 10.53730/ijhs.v6ns4.10527.
62. Salmons, Harold I., Ashley N. Payne, Michael J. Taunton, Aaron R. Owen, Kristin M. Fruth, Daniel J. Berry, and Matthew P. Abdel. 2023. "Nonsteroidal Anti-Inflammatory Drugs and Oral Corticosteroids Mitigated the Risk of Arthrofibrosis After Total Knee Arthroplasty." *Journal of Arthroplasty*. doi: 10.1016/j.arth.2023.03.076.
63. Samiraninezhad, Nazafarin, Mostafa Rezaee, Ahmad Gholami, Ali Amanati, and Maryam Mardani. 2023. "A Novel Chitosan-Based Doxepin Nano-Formulation for Chemotherapy-Induced Oral Mucositis: A Randomized, Double-Blinded, Placebo-Controlled Clinical Trial." *Inflammopharmacology*. doi: 10.1007/s10787-023-01325-7.
64. Selmin, Francesca, Silvia Franzè, Antonella Casiraghi, and Francesco Cilurzo. 2022. "Spotlight on Calcipotriol/Betamethasone Fixed-Dose Combination in Topical Formulations: Is There Still Room for Innovation?" *Pharmaceutics*.
65. Shalaby, Rodayna Atef, Omaima El-Gazayerly, and Mohammed Abdallah. 2022. "Cubosomal Betamethasone-Salicylic Acid Nano Drug Delivery System for Enhanced Management of Scalp Psoriasis." *International Journal of Nanomedicine*. doi: 10.2147/IJN.S345430.
66. Sharapova, E. P., E. A. Taskina, N. G. Kashevarova, L. I. Alekseeva, and A. M. Lila. 2021. "Efficacy of Chondroitin Sulfate in Patients with Knee and Hip Osteoarthritis." *Sovremennaya Revmatologiya*. doi: 10.14412/1996-7012-2021-4-120-125.
67. Šléglová, Olga. 2023. "Pain Treatment Options for Osteoarthritis." *Vnitrni Lekarstvi*. doi: 10.36290/vnl.2023.019.
68. Sobhani, Kaivon, Jinlei Li, and Milaurise Cortes. 2023. "Nonsteroidal Anti-Inflammatory Drugs (NSAIDs)." in *First Aid Perioperative Ultrasound: Acute Pain Manual for Surgical Procedures*.
69. Srividya, G., R. A. M. Jainaf Nachiya, Doaa Ebrahim, Aida M. El-Sagheer, Saminathan Kayarohanam, Ashok Kumar Janakiraman, Jiyauddin Khan, and Jamal Moideen Muthu Mohamed. 2022. "COMPARATIVE STUDY OF SEMI-SOLID BASES OF NAPROXEN: PHARMACEUTICAL TECHNOLOGY ASPECTS." *International Journal of Applied Pharmaceutics*. doi: 10.22159/ijap.2022.v14ti.38.
70. Tam, Samantha, Grace Zhou, Mark Trombetta, Saverio Caini, Julie Ryan Wolf, Corina van den Hurk, Mara Beveridge, Henry Lam, Pierluigi Bonomo, Edward Chow, and Tara Behroozian. 2023. "Topical Corticosteroids for the Prevention of Severe Radiation Dermatitis: A Systematic Review and Meta-Analysis." *Supportive Care in Cancer*.
71. Timotijević, Mirjana D., Tanja Ilić, Bojan Marković, Danijela Randjelović, Nebojša Cekić, Ines Nikolić, Snežana Savić, and Ivana Pantelić. 2022. "Coupling AFM, DSC and FT-IR towards Elucidation of Film-Forming Systems Transformation to Dermal Films: A Betamethasone Dipropionate Case Study." *International Journal of Molecular Sciences*. doi: 10.3390/ijms23116013.

72. Wang, Xiangxiang, Shuang He, Kaiye Wang, Xin Wang, Tingyuan Yan, Tingxuan Yan, and Zhixiang Wang. 2023. "Fabrication of Betamethasone Micro- and Nanoparticles Using Supercritical Antisolvent Technology: In Vitro Drug Release Study and Caco-2 Cell Cytotoxicity Evaluation." *European Journal of Pharmaceutical Sciences*. doi: 10.1016/j.ejps.2022.106341.
73. Wang, Xiaoyi, Quanying Bao, Min Sung Suh, Michail Kastellorizios, Ruifeng Wang, and Diane J. Burgess. 2022. "Novel Adapter Method for in Vitro Release Testing of in Situ Forming Implants." *International Journal of Pharmaceutics*. doi: 10.1016/j.ijpharm.2022.121777.
74. Wang, Yang, Guoqing Li, Muhtar Momin, Baochao Ji, Li Cao, and Aishajiang Aisikeerbayi. 2022. "Comparison of Different Local Analgesia Protocols in Postoperative Pain Management after Total Knee Arthroplasty." *Brazilian Journal of Anesthesiology (English Edition)*. doi: 10.1016/j.bjane.2020.12.020.
75. Wang, Yuanyuan, Mahnuma Mahfuz Estee, Desmond Gan, Yuan Z. Lim, Stephane Heritier, Anita E. Wluka, Sultana Monira Hussain, Natalie L. Trevaskis, and Flavia M. Cicuttini. 2023. "Effect of 6-Week Treatment with Topical Betamethasone Dipropionate in Patients with Symptomatic Hand Osteoarthritis: A Randomized Double-Blind, Placebo-Controlled Trial." *Osteoarthritis and Cartilage Open*. doi: 10.1016/j.ocarto.2023.100382.
76. Wibrianto, Aswandi, Dinar F. Putri, Satya C. W. Sakti, Hwei V. Lee, and Mochamad Z. Fahmi. 2021. "Naproxen Release Aspect from Boron-Doped Carbon Nanodots as a Bifunctional Agent in Cancer Therapy." *RSC Advances*. doi: 10.1039/d1ra06148h.
77. Yang, Hui, Lin Wang, Xiao Chu, Xiaojuan Shi, Xinhe Li, and Tieshan Li. 2022. "BoNT/A Alleviates Neuropathic Pain in Osteoarthritis by down-Regulating the Expression of P2X4R in Spinal Microglia." *Toxicon*. doi: 10.1016/j.toxicon.2021.12.012.
78. Yang, Li, Shuang Wang, Zhongshui Xie, Rongrong Xing, Runqin Wang, Xuan Chen, and Shuang Hu. 2023. "Deep Eutectic Solvent - Loaded Fe3O4@MIL-101(Cr) with Core–Shell Structure for the Magnetic Solid Phase Extraction of Non-Steroidal Anti-Inflammatory Drugs in Environmental Water Samples." *Microchemical Journal*. doi: 10.1016/j.microc.2022.108150.
79. Yang, Yahua, Zhizhong Xue, Ran Meng, Zhe Wu, Zhaojia Li, Wei Zhang, and Shihui Ge. 2022. "Determination of Eight Kinds of Glucocorticoids Residues in Chicken Muscle with On-Line Clean up Combined HPLC-MS/MS." *Acta Chromatographica*. doi: 10.1556/1326.2021.00933.
80. Ye, Zhihong, Roger Oriol, Chao Yang, Ignasi Sirés, and Xiao Yan Li. 2022. "A Novel NH2-MIL-88B(Fe)-Modified Ceramic Membrane for the Integration of Electro-Fenton and Filtration Processes: A Case Study on Naproxen Degradation." *Chemical Engineering Journal*. doi: 10.1016/j.cej.2021.133547.
81. Yeganeh, Faten Eshrati, Amir Eshrati Yeganeh, Mohammad Yousefi, Bahareh Farasati Far, Iman Akbarzadeh, Dmitry Olegovich Bokov, Kaamran Raahemifar, and Madjid Soltani. 2022. "Formulation and Characterization of Poly (Ethylene Glycol)-Coated Core-Shell Methionine Magnetic Nanoparticles as a Carrier for Naproxen Delivery: Growth Inhibition of Cancer Cells." *Cancers*. doi: 10.3390/cancers14071797.
82. Zare, Masoud Habibi, and Arjomand Mehrabani-Zeinabad. 2022. "Photocatalytic Activity of ZrO2/TiO2/Fe3O4 Ternary Nanocomposite for the Degradation of Naproxen: Characterization and Optimization Using Response Surface Methodology." *Scientific Reports*. doi: 10.1038/s41598-022-14676-y.
83. Zemánková, Alžběta, Fatima Hassouna, Martin Klajmon, and Michal Fulem. 2023. "Solid–Liquid Equilibrium in Co-Amorphous Systems: Experiment and Prediction." *Molecules*. doi: 10.3390/molecules28062492.
84. Zhou, Jun, Zhiyuan Bao, Panpan Wu, and Chao Chen. 2021. "Preparation and Synthetic Application of Naproxen-Containing Diaryliodonium Salts." *Molecules*. doi: 10.3390/molecules26113240.